The Meteoritical Society

Meteoritics & Planetary Science 51, Nr 7, 1268–1288 (2016)
doi: 10.1111/maps.12663

Petrogenesis of the Northwest Africa 4898 high-Al mare basalt

Shaolin LI[1], Weibiao HSU[1,2*], Yunbin GUAN[3], Linyan WANG[4], and Ying WANG[1]

[1]Key Laboratory of Planetary Sciences, Purple Mountain Observatory, Chinese Academy of Sciences, Nanjing 210008, China
[2]Institute of Space Sciences, Macau University of Science and Technology, Macau, China
[3]Division of Geological and Planetary Sciences, California Institute of Technology, Pasadena, California 91125, USA
[4]Faculty of Earth Sciences, China University of Geosciences, Wuhan 430074, China
[*]Corresponding author. E-mail: wbxu@pmo.ac.cn

(Received 15 June 2015; revision accepted 30 March 2016)

Abstract–Northwest Africa (NWA) 4898 is the only low-Ti, high-Al basaltic lunar meteorite yet recognized. It predominantly consists of pyroxene (53.8 vol%) and plagioclase (38.6 vol %). Pyroxene has a wide range of compositions ($En_{12–62}Fs_{25–62}Wo_{11–36}$), which display a continuous trend from Mg-rich cores toward Ca-rich mantles and then to Fe-rich rims. Plagioclase has relatively restricted compositions ($An_{87–96}Or_{0–1}Ab_{4–13}$), and was transformed to maskelynite. The REE zoning of all silicate minerals was not significantly modified by shock metamorphism and weathering. Relatively large (up to 1 mm) olivine phenocrysts have homogenous inner parts with Fo ~74 and sharply decrease to 64 within the thin out rims (~30 μm in width). Four types of inclusions with a variety of textures and modal mineralogy were identified in olivine phenocrysts. The contrasting morphologies of these inclusions and the chemical zoning of olivine phenocrysts suggest NWA 4898 underwent at least two stages of crystallization. The aluminous chromite in NWA 4898 reveals that its high alumina character was inherited from the parental magma, rather than by fractional crystallization. The mineral chemistry and major element compositions of NWA 4898 are different from those of 12038 and Luna 16 basalts, but resemble those of Apollo 14 high-Al basalts. However, the trace element compositions demonstrate that NWA 4898 and Apollo 14 high-Al basalts could not have been derived from the same mantle source. REE compositions of its parental magma indicate that NWA 4898 probably originated from a unique depleted mantle source that has not been sampled yet. Unlike Apollo 14 high-Al basalts, which assimilated KREEPy materials during their formation, NWA 4898 could have formed by closed-system fractional crystallization.

INTRODUCTION

Since the Apollo missions, the lunar magma ocean (LMO) concept emerged to the forefront and gained wide support from both post-Apollo missions and laboratory investigations of lunar materials (e.g., Shearer et al. [2006] and references therein). Immediately following the initial accretion, the Moon experienced a planetary-scale differentiation facilitated by a lunar magma ocean. Crystallization of the LMO produced mafic lithologies that sank to form the lunar mantle (e.g., Warren 1985; Snyder et al. 1992; Elardo et al. 2011). As solidification proceeded, less dense plagioclase crystallized and floated to the top to form a primary lunar crust (e.g., Taylor and Jakes 1974). Rocks from the lunar highlands "crust" are essentially anorthositic in composition and very ancient (4.3–4.5 Gyr; Borg et al. 1999, 2011; Norman et al. 2003; Nyquist et al. 2002). Partial melting of deep, mafic cumulates generated a wide variety of mare basalts that primarily fill impact basins and irregular depressions on the lunar near side. Studies also reveal the existence of a group of plutonic and volcanic rocks that recorded the magmatic events of the post-LMO lunar magmatic activity. Representative lithologies include high-Mg suites, alkali-rich suites, KREEP basalts, high-K basalts, and high-Al basalts (Warner et al. 1976; Warren and Wasson 1979; Hess 1994; Shearer and Papike 2005; Shearer et al. 2006; Elardo et al. 2011, 2012).

High-Al basalts (>11 wt% Al_2O_3) were first recognized in the Apollo 14 collection (Ridley 1975; Taylor et al. 1983). They have relatively uniform major element compositions but exhibit a wide range (a factor of eight) of incompatible trace element concentrations (Dickinson et al. 1985; Neal and Kramer 2006). The Apollo 14 high-Al basalts are the oldest lunar basalts and have ages that range from 3.9 to 4.3 Ga (Papanastassiou and Wasserburg 1971; Dasch et al. 1987; Nyquist and Shih 1992). The Luna 16 mission also returned high-Al basalts (Albee et al. 1972), but they are much younger (~3.4 Ga; Papanastassiou and Wasserburg 1972). In addition, one Apollo 12 sample, 12038, also has high-Al signatures with an age of ~3.3 Ga, which was classified as a feldspathic basalt (Nyquist et al. 1979, 1981; Neal et al. 1994). Initial isotope ratios, mineral chemistry, trace element abundances, and crystallization ages require that high-Al basalts were derived from different source regions during distinct lunar magmatic events (e.g., Hagerty et al. 2005; Neal and Kramer 2006; Shearer et al. 2006; Hui et al. 2013).

Lunar meteorites, being the random samples ejected from the lunar surface by impact, provide additional information on lunar differentiation and evolution. Among all basaltic meteorites so far identified, Northwest Africa (NWA) 4898 contains 12 wt% Al_2O_3 and displays an affinity to the Apollo 14 high-Al basalts (Greshake et al. 2008). However, NWA 4898 is younger than other high-Al basalts (~3.6 Ga; Fernandes et al. 2009; Gaffney et al. 2008) and has the highest $^{147}Sm/^{144}Nd$ ratio among mare basalts, suggesting that it may have been derived from the most isotopically depleted mantle source (Gaffney et al. 2008). Here, we report the petrology, mineral chemistry, and trace element compositions of NWA 4898, and provide additional constraints on its petrogenesis as well as the lunar evolution.

ANALYTICAL METHODS

A slice of 0.332 g NWA 4898 was acquired from Stefan Ralew. Two polished sections (PMO-0204, -0205) were made, with a total exposed area ~1 cm^2. The sections were first examined with a Nikon E400POL optical microscope. The mineralogy, texture, and petrography of NWA 4898 were further characterized using a Hitachi S-3400N scanning electron microscope equipped with an Oxford INCA 7021 energy dispersive spectroscope (EDS). Modal abundances were estimated from backscattered electron (BSE) images and elemental maps by pixel-counting using the phase map function within Oxford INCA software, assuming that area fractions were equal to volume percentages.

We determined the major and minor element concentrations of minerals, glasses, and shock-melt veins using a JEOL JXA-8100M electron microprobe (EMP) at the China University of Geosciences, Wuhan. For olivine, pyroxene, and oxide analyses, the EMP was operated at a 15 keV accelerating voltage with a focused beam (1 μm) of 20 nA current. Plagioclase and glass phases were analyzed with a 15 keV accelerating voltage, a 10 nA beam current, and a defocused beam (5 and 10 μm, respectively). Counting times were 20 s for all elements. Both synthetic and natural mineral standards were used, and matrix corrections were based on ZAF procedures (Armstrong 1982).

Concentrations of minor and trace elements were measured in situ in olivine, pyroxene, plagioclase, melt inclusions, and shock-melt veins with the Cameca 7f-Geo ion microprobe at Caltech, using a similar instrumental setup as described by Hsu et al. (2004). An O^- primary ion beam was accelerated to −12.5 keV. Primary beam currents of 5 nA for pyroxene and glass and 10 nA for olivine and plagioclase were focused on the samples over spot diameters of 10–15 μm. Secondary ions, offset from a nominal +10 keV accelerating voltage by −80 eV, were collected in peak-jumping mode with an electron multiplier (EM). Ratios of measured intensities (e.g., element/$^{30}Si^+$) were normalized to SiO_2 concentrations derived from electron microprobe analyses. Natural mineral and synthetic glass standards were used to determine the sensitivity factors. The analytical errors reported are based on counting statistics only.

Crystallization sequences of NWA 4898 were derived from a combination of modeling using the MELTS program and petrographic observations (Ghiorso and Sack 1995; Asimow and Ghiorso 1998). The parameters of starting temperature, pressure, and oxygen fugacity in the MELTS program were set to 1350 °C, 10 kbar, and −13.5 log f_{O2}, respectively. The program then was allowed to run until the magma had completely crystallized and ending pressure being 1 kbar.

RESULTS

Petrography

NWA 4898 was found in northwest Africa in 2007. The original mass of the meteorite was 137 g and it is almost completely covered with a fusion crust. This meteorite is a fine-grained, subophitic/ophitic-textured mare basalt (Fig. 1a). Small chemically zoned pyroxene grains (~50 μm) are intergrown with plagioclase laths (up to 200 μm in length), but they are not poikilitically enclosed. Euhedral chromite (up to

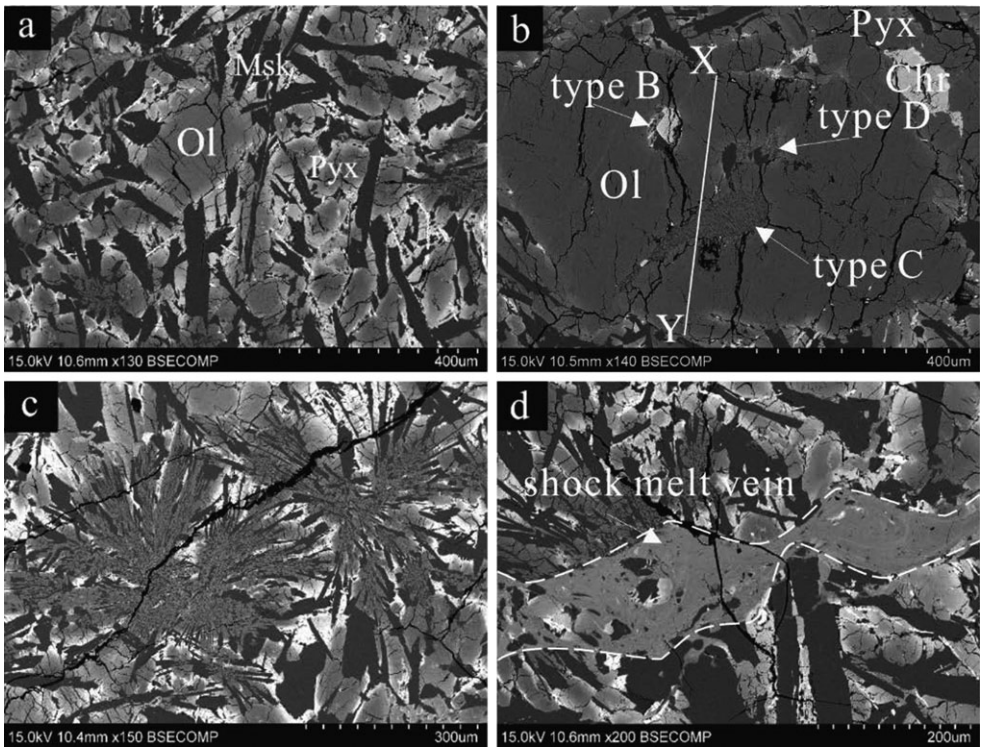

Fig. 1. Backscattered electron (BSE) images of NWA 4898. a) Euhedral olivine (Ol), pyroxene (Pyx), and maskelynite (Msk) in the groundmass. Plagioclase was transformed to maskelynite due to shock metamorphism. b) Olivine phenocrysts often contain different inclusions that were entrapped at different crystallization stages. The compositional profile displayed in Fig. 5 from X to Y is labeled. c) Variolitic texture composed of sprays of pyroxene and plagioclase. d) A shock-induced melt vein (outlined by dashed line) with flow-banded schlieren, eroded mineral fragments.

150 μm) occurs interstitially between mafic minerals, and acicular ilmenite (up to 150 μm in length) often crosscuts pyroxene and plagioclase grains. Relatively large (up to 1 mm) euhedral to subhedral olivine grains, with or without pyroxene reaction rims, are present as phenocrysts (Fig. 1a) and often contain different types of inclusions (Figs. 1b and 2; see Mineral Chemistry section for inclusion descriptions). Many inclusions have cracks around them, perhaps because the inclusions represent weak spots in the olivine and promote cracking during shock. Variolitic textures composed of sprays of pyroxene and plagioclase are ubiquitous in the groundmass (Fig. 1c). Plagioclase grains in the olivine inclusions and the groundmass were transformed to maskelynite due to the shock effects. Several shock-induced melt veins (5–200 μm in width) are visible along or cutting through mineral grain boundaries (Fig. 1d). These veins are rich in flow-banded schlieren and contain eroded mineral fragments of pyroxene, maskelynite, and chromite.

The area-weighted mean of modal analyses on the two polished sections of NWA 4898 (~1 cm^2) is given in Table 1. Data for Apollo 14 and other high-Al basalts are also listed for comparison. NWA 4898 is predominantly composed of pyroxene (53.8 vol%) and plagioclase (38.6 vol%) with minor olivine (5 vol%) and opaque phases (2.5 vol%). The most abundant opaque phase is ilmenite, followed by chromite. Phosphate and Zr-rich mineral phases were not found in the sections.

Mineral Chemistry

Pyroxene grains are chemically zoned from Mg-rich cores toward Ca-rich mantles and then to Fe-rich rims ($Fs_{26–62}Wo_{9–35}En_{12–62}$; Fig. 3; Tables 2 and 3). Pyroxene grains surrounded by late-stage minerals (e.g., ilmenite) are relatively Fe-rich, but no pyroxferroite was found. In these areas, minerals were extensively fractured because of shock metamorphism. Rare earth elements (REE) in pyroxene exhibit a HREE-enriched pattern with a negative Eu anomaly (Fig. 4a; Table 4). In the pyroxene core, the slope of LREE is steeper than that of HREE, with $(La/Sm)_N$ being 10 times of $(Gd/Lu)_N$ (subscript "N" means CI chondrite normalized with data from Anders and Grevesse 1989). But in the rim, this ratio decreases to ~2. The REE abundances of the rim are also higher than those of the Mg-rich core by an average factor of 2.

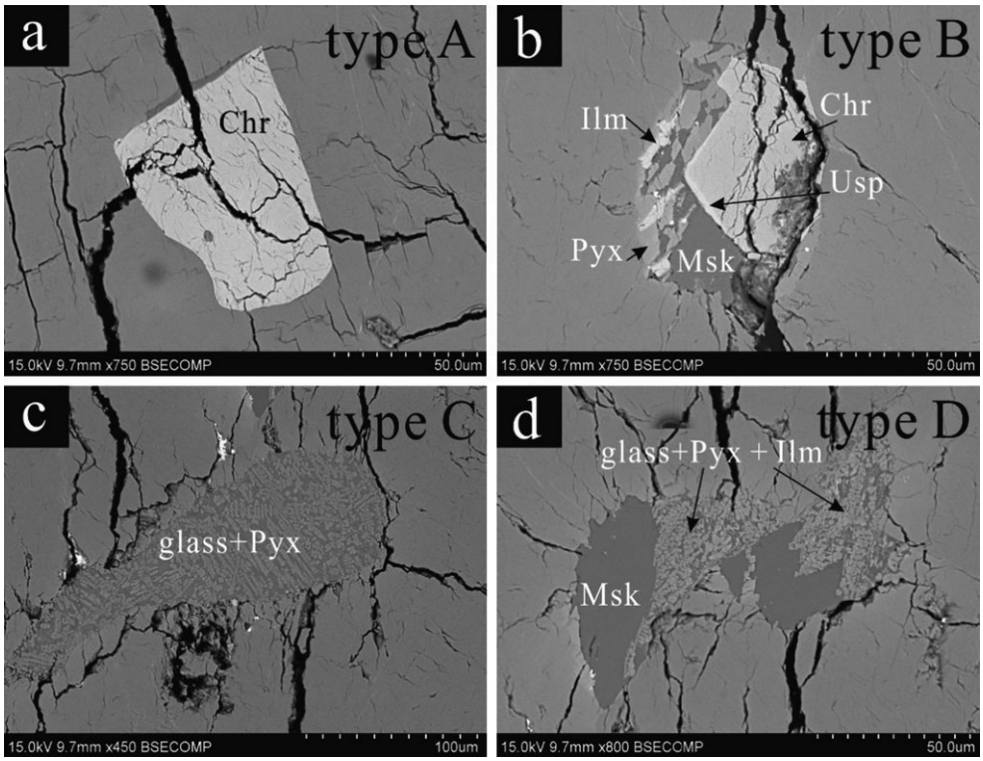

Fig. 2. Four types of olivine inclusions. Type B (b), type C (c), and type D (d) inclusions are enlarged photos from Fig. 1b, while the type A inclusion in panel (a) is from another olivine phenocryst. Phase abbreviations: Ol = olivine; Pyx = pyroxene; Msk = maskelynite; Chr = chromite; Ilm = ilmenite; Usp = ulvöspinel.

Table 1. Modal abundances (vol%) in high-Al mare basalts.

		14321[a]					Luna 16[d]		
	NWA 4898	Granulated	Subophitic	Ophitic	14053[b]	14072[c]	B-1	60053,2-9[e]	12038[f]
Olivine	5.1	0–10	0–8	3–16	2.8	2.5	Minor		0.1
Pyroxene	53.8	25–45	35–52	16–38	48.1	49.9	50	50	48.8
Plagioclase	38.6	20–45	20–40	18–35	40.5	38.3	40	25	43.8
Ilmenite	2.3	6–12	10–16	5–15	3.3	7.7	7	6	3.5
Chromite	0.2	0–8	0–5	0–5	0.3		Minor		0.2
FeNi/Troilite	Trace	1–9	1–6	2–11	0.4		Minor	Trace	
SiO_2	Trace	0–5	0–3	0–6	2.4	1.7		6	2.7
Glass		2–22	0–6	2–20	0.9			Trace	0.7

Reference sources: a) Neal et al. (1989a); b) Taylor et al. (2004); c) Longhi et al. (1972); d) Albee et al. (1972); e) Zeigler et al. (2006); f) Neal et al. (1994).

Plagioclase was entirely transformed to maskelynite due to shock metamorphism. The grains occur as subhedral tabular to blocky crystals with varying compositions ($An_{87–96}Or_{0–1}Ab_{4–13}$). They are commonly zoned from a Ca-rich core to a Na-rich rim (Tables 2 and 3). There is 0.36–1.88 wt% FeO in maskelynite of NWA 4898 and FeO content has a negative correlation with CaO content statistically. The REE pattern of maskelynite exhibits a negative slope with a large positive Eu anomaly (Fig. 4b; Table 4).

Olivine occurs as phenocrysts or individual grains in the groundmass. Phenocrysts are nearly homogeneous from the core to the inner rim (~200 μm from the center), with Fo varying from 74 to 72. But Fo decreases sharply within the thin outer rim (~30 μm in width), from ~70 to 55 (Fig. 5; Tables 2 and 3). CaO content varies along with Fo, which shows an apparent increase in the outer rim. Ni content decreases generally from the core (74 ± 2 ppm) to the rim (54 ± 1 ppm) of olivine phenocrysts. However, their REE abundances, like the major elements, are relatively constant from the core to the inner rim, yet increase nearly seven times in the outer rim (Fig. 4c). Y and Zr contents are enriched by a factor of 15–31 in the outer rim (0.31–4.57 ppm

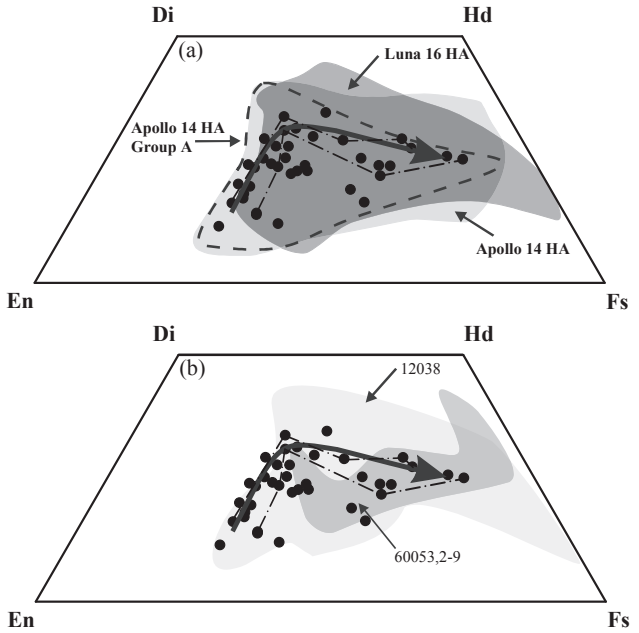

Fig. 3. Enstatite–diopside–hedenbergite–ferrosilite pyroxene quadrilateral for NWA 4898 (black dots). Pyroxene compositions of Apollo 14 and Luna 16 high-Al basalts (a), as well as 12038 and 60053,2-9 (b) are plotted for comparison. Two dash-dot lines represent profiles from core to rim of two different pyroxene grains in NWA 4898. The large curved arrow represents the evolution trend of pyroxene in NWA 4898. The dashed line in panel (a) represents the pyroxene compositional range of Apollo 14 Group A high-Al basalts. Data for Apollo 14 high-Al basalts are taken from Shervais et al. (1985), Neal et al. (1988, 1989a); those for Luna 16 high-Al basalts are taken from Albee et al. (1972) and Kurat et al. (1976); those for 12038 are taken from Beaty et al. (1979); and those for 60053,2-9 are from Zeigler et al. (2006). Pyroxene compositions in NWA 4898 are quite similar to those in Apollo 14 Group A high-Al basalts. They do not show an evolutionary trend to Fe-rich pyroxferroite as seen in 12038 and Luna 16 high-Al basalts.

for Y, 0.17–5.4 ppm for Zr; Table 4). Individual olivine grains in the groundmass are often intergrown with ilmenite (Fig. 1a) and have Fo ranging from 44 to 67 (Table 3).

Ilmenite is the most abundant opaque phase in NWA 4898. It occurs as acicular skeletal crystals in the mesostasis. Ilmenite is almost pure $FeTiO_3$, with minor MgO (<0.2 wt%) and MnO (<0.4 wt%; Table 3).

Spinel is the second most abundant opaque mineral and occurs as euhedral inclusions in olivine, pyroxene, and maskelynite, or exists in the groundmass as individual or clusters of grains. The average Al_2O_3 content of the early formed chromite in NWA 4898 is ~19 wt% (Table 3). Spinel usually has an Al-Ti-chromite core and a Cr-ulvöspinel rim with a sharp boundary. Compositions of Al-Ti-chromite and Cr-ulvöspinel vary in a limited range respectively, forming a conspicuous gap between two phases (Fig. 6). Spinel grains completely enclosed in olivine and Mg-rich pyroxene are Al-Ti-chromite, displaying slightly gradational zoning from a Cr-rich core to a Ti-rich rim. Partially enclosed spinels usually show gradational zoning to the enclosed side and a sharp boundary to the other, nearly uniform Cr-ulvöspinel. Al-Ti-chromite grains in the mesostasis or enclosed in Fe-rich pyroxene and maskelynite also have sharp boundaries with Cr-ulvöspinel rims.

Four types of inclusions are observed in olivine phenocrysts (Figs. 1b and 2). Type A inclusions are phaneritic and contain only opaque minerals, including Al-Ti-chromite or Fe,Ni-metal or both (Fig. 2a). Type B inclusions (35–80 μm) are often cut by numerous fractures and also phaneritic, containing pyroxene, maskelynite, ilmenite, Fe,Ni-metal, and Al-Ti-chromite mantled by Cr-ulvöspinel (Fig. 2b). In most cases, only maskelynite and pyroxene are present. Type C inclusions (50–150 μm) are glassy with pyroxene and ilmenite crystals (Fig. 2c). Type D inclusions (40–90 μm) are relatively rare and are texturally between types B and C (Fig 2d). Maskelynite (20–40 μm) and nearly equal volume of glass with pyroxene and ilmenite crystals are all observed in type D inclusions. The outlines of type B and C inclusions are usually irregular but smooth (e.g., embayed or bulb-like), whereas type D inclusions are usually angular and defined by crystallized minerals. The composition of mineral grains in different types of inclusions varies. Maskelynite in type B has a narrow range ($An_{90–93}$) compared to that in type D ($An_{88–96}$); the composition of which overlaps almost all maskelynite in NWA 4898 (Fig. 7). The composition of pyroxene in type B also exhibits a restricted range ($Fs_{21–45}$; Fig. 7). Even though a defocused beam (10 μm) was used, the major element compositions of type C melt inclusions vary moderately. For example, SiO_2 content varies from 47.5 to 52.9 wt% with most close to 50 wt%. Compared to the bulk rock, the type C melt inclusions are enriched in CaO (13–16 wt%), Al_2O_3 (13–15 wt%), and TiO_2 (2.1–4.1 wt%) but depleted in MgO (1.3–4.5 wt%) and Cr_2O_3 (0.01–0.16 wt%). Mg# (Mg/[Mg+Fe]) varies from 0.19 to 0.38, with an average of 0.28, which is much lower than that of the bulk rock (0.46; Table 5). However, their trace element compositions are quite homogeneous (Fig. 4d). The REE patterns of type C melt inclusions are nearly the same as those of bulk rock and shock-induced veins, but at slightly higher levels (Fig. 4d; Table 6). Although type C melt inclusions are partially crystallized, the pyroxene and ilmenite crystals are as small as ~1 μm and homogeneously distributed (Fig. 2c). The beam size of SIMS analyses used on type C melt inclusions is ~15 μm. Therefore, the results

Table 2. Compositional variations of major mineral phases in high-Al mare basalts.

			Apollo 14[a]						
		NWA 4898	Group A	Group B	Group C	14072[b]	Luna 16[c]	60053,2-9[d]	12038[e]
Olivine	Fo	44.5–74.0	38.9–78.1	55.7–73.0	61.3–71.2	30–79	45–72		<10, 60
Pyroxene	En	12.4–62.0	14.5–60.3	4.6–66.6	16.3–61.8	16–65	1–55	4–45	3–62
	Fs	25.5–62.6	21.2–59.3	20.8–72.1	24.3–50.9	23–62	28–85	34–63	24–83
	Wo	9.9–36.4	9.1–38.5	4.4–39.7	9.3–36.2	5–38	7–46	18–42	10–39
Plagioclase	An	89.2–96.0	81.1–96.8	77.0–95.2	85.3–93.4		83–93	88–94	73–82
	Ab	4.0–10.0	3.0–16.8	4.6–19.8	6.3–13.0		7–13	5–10	14–20
	Or	0.0–0.9	0.1–2.8	0.2–13.2	0.1–1.7		2–4	0.1–1.4	0.3–2

Reference sources: a) Dickinson et al. (1985), Group A represents Group 4 and Group 5, Group B represents Group 1 and Group 2, Group C represents Group 3, as suggested by Neal and Kramer (2006); b) Longhi et al. (1972) and McGee et al. (1977); c) Kurat et al. (1976); d) Zeigler et al. (2006); e) Keil et al. (1971) and Beaty et al. (1979).

Table 3. Representative electron microprobe analyses (wt%) of minerals in NWA 4898.

	Pyroxene			Maskelynite			Olivine phenocryst					Spinel	
Oxide	Core	Rim		Core	Rim		Core	Mantle	Rim	Olivine in the groundmass	Ilmenite	Al-Ti-chromite	Cr-ulvöspinel
SiO_2	52.36	47.38		46.85	49.69		37.58	36.99	34.99	34.86	0.24	0.36	0.36
TiO_2	0.69	2.02		0.06	0.07		0.05	0.06	0.12	0.17	51.83	2.52	24.29
Al_2O_3	2.64	2.10		32.32	29.93		0.07	0.11	0.08	0.09	0.07	19.76	5.74
Cr_2O_3	0.98	0.09		0.01	bd		0.31	0.26	0.02	0.04	0.03	42.87	15.60
FeO	16.28	28.18		0.44	0.69		23.47	25.18	37.94	39.12	46.95	24.29	49.97
MnO	0.26	0.35		bd	bd		0.25	0.28	0.34	0.32	0.31	0.25	0.30
MgO	21.29	6.65		0.36	0.51		37.54	36.28	25.68	25.04	0.08	8.65	3.13
CaO	5.48	12.89		18.61	17.49		0.29	0.4	0.41	0.32	0.40	0.02	0.09
Na_2O	0.02	0.03		0.51	1.01		bd	bd	bd	0.03	0.03	0.01	bd
K_2O	bd	bd		0.01	0.01		bd	bd	bd	0.02	bd	bd	0.01
Total	99.98	99.69		99.16	99.39		99.56	99.56	99.57	99.99	99.95	98.73	99.50
En	62.0	21.0	An	95.2	90.5	Fo	74	72	55	53	Chr	55.6	22.2
Fs	26.6	49.8	Ab	4.7	9.5	Fa	26	28	45	47	Her	38.2	12.3
Wo	11.5	29.2	Or	0.1	0.1						Ulv	6.2	65.7

bd = below detection limit.
Completed data are available in Tables S1–S5 in supporting information.

could closely represent the average compositions of type C melt inclusions. This is further illustrated in Fig. 4d that the REE compositions of two analyses on two different type C melt inclusions are nearly identical. Completed major and trace element data for type C melt inclusions are available in Tables S5 and S7 in supporting information.

Bulk Rock Composition

Due to the small specimen we hold, bulk analysis of NWA 4898 was not carried out here. The average compositions (23 EMP analyses) of shock-melt veins are presented in Table 5, and the data for the bulk rock (Greshake et al. 2008) are also listed for comparison. The compositions of shock-melt veins are highly heterogeneous with regard to major and minor elements but quite homogenous in REE, with relative standard deviation of 3–13% for major elements, 15–59% for minor elements, but only 1–7% for REE. The shock-melt veins yield an average composition close to the data reported by Greshake et al. (2008) except for MgO and Cr_2O_3. MgO (6.70 wt%) and Cr_2O_3 (0.27 wt%) contents of shock-melt veins are significantly lower than those of bulk rock (8.31 wt% and 0.43 wt%, respectively). FeO and MnO contents also show minor depletions, whereas other major elements (e.g., SiO_2 and Al_2O_3) exhibit a small enrichment over the bulk rock compositions. These data indicate that the refractory phase of spinel did not completely melt. Therefore, whole rock major element compositions from Greshake et al. (2008) for NWA 4898 are used here (Table 5). Based on the classification scheme of Neal and Taylor (1992), NWA 4898 can be classified as a low-Ti, high-Al basalt.

The average REE abundances of shock-melt veins are slightly lower than those of the whole rock analyzed by Greshake et al. (2008), but their REE patterns are

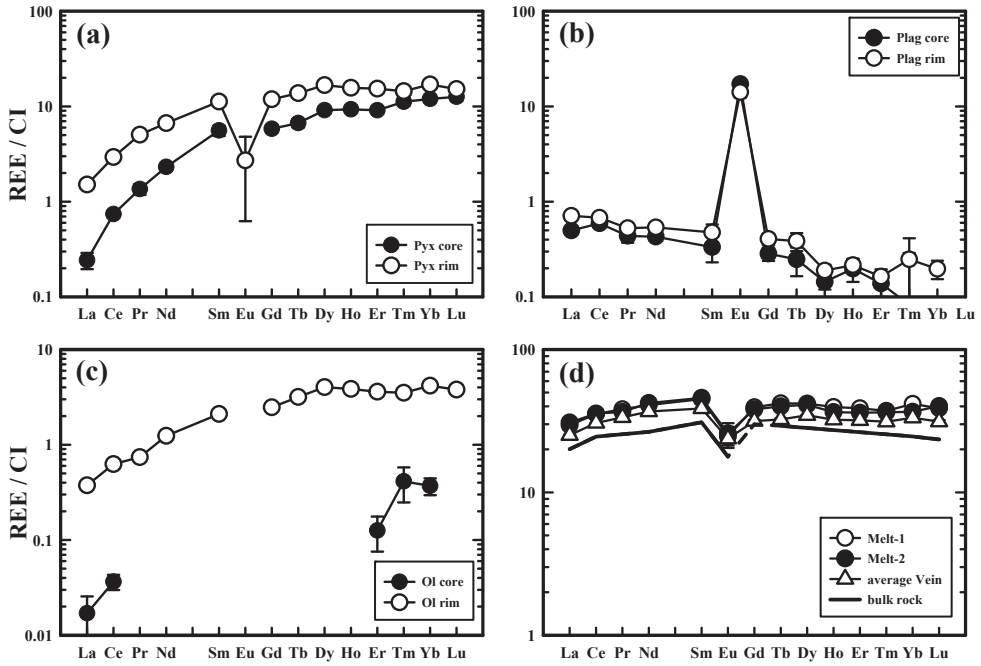

Fig. 4. Representative chondrite-normalized (Anders and Grevesse 1989) REE patterns for pyroxene (a), plagioclase (b), olivine (c), as well as for type C melt inclusions, average shock-induced veins, and the bulk rock of NWA 4898 (d). Melt 1 and Melt 2 in Fig. 4d are two analyses on two different melt C inclusions.

Table 4. Representative trace element compositions (ppm) of minerals in NWA 4898.

	Olivine		Pyroxene		Maskelynite	
	Core	Rim	Core	Rim	Core	Rim
Sc	14.6 ± 0.2	35.5 ± 0.3	133.1 ± 0.8	172.3 ± 0.9	12.8 ± 0.1	10.1 ± 0.1
Ni	74 ± 2	54 ± 1	122 ± 3	202 ± 4	167 ± 1	126 ± 2
Y	0.32 ± 0.02	4.58 ± 0.06	13.0 ± 0.2	29.2 ± 0.3	0.216 ± 0.009	0.24 ± 0.01
Zr	0.17 ± 0.02	5.4 ± 0.1	9.0 ± 0.2	46.1 ± 0.5	0.064 ± 0.007	0.037 ± 0.007
Ba	9.3 ± 0.1	21.7 ± 0.2	0.55 ± 0.05	4.6 ± 0.1	9.13 ± 0.07	9.51 ± 0.09
La	0.004 ± 0.002	0.082 ± 0.008	0.06 ± 0.01	0.58 ± 0.04	0.133 ± 0.007	0.17 ± 0.01
Ce	0.020 ± 0.004	0.35 ± 0.02	0.44 ± 0.03	2.58 ± 0.08	0.36 ± 0.01	0.41 ± 0.02
Pr	bd	0.062 ± 0.006	0.12 ± 0.02	0.52 ± 0.03	0.045 ± 0.004	0.047 ± 0.005
Nd	bd	0.52 ± 0.03	1.04 ± 0.08	3.6 ± 0.1	0.22 ± 0.01	0.24 ± 0.02
Sm	bd	0.29 ± 0.04	0.8 ± 0.1	2.1 ± 0.2	0.05 ± 0.01	0.07 ± 0.02
Eu	bd	bd	bd	0.23 ± 0.09	0.77 ± 0.08	0.8 ± 0.1
Gd	bd	0.45 ± 0.04	1.1 ± 0.1	3.2 ± 0.2	0.059 ± 0.008	0.08 ± 0.01
Tb	bd	0.11 ± 0.01	0.24 ± 0.03	0.68 ± 0.04	0.007 ± 0.002	0.014 ± 0.003
Dy	bd	0.91 ± 0.04	2.19 ± 0.09	5.0 ± 0.1	0.049 ± 0.006	0.046 ± 0.007
Ho	bd	0.20 ± 0.01	0.51 ± 0.03	1.07 ± 0.05	0.012 ± 0.002	0.012 ± 0.002
Er	0.019 ± 0.007	0.53 ± 0.03	1.43 ± 0.07	3.2 ± 0.1	0.025 ± 0.004	0.026 ± 0.005
Tm	0.010 ± 0.004	0.080 ± 0.009	0.27 ± 0.03	0.53 ± 0.04	0.007 ± 0.004	0.006 ± 0.004
Yb	0.06 ± 0.01	0.63 ± 0.04	1.9 ± 0.1	4.1 ± 0.2	0.019 ± 0.004	0.032 ± 0.007
Lu	0.086 ± 0.002	0.02 ± 0.01	0.30 ± 0.03	0.53 ± 0.04	bd	bd

bd = below detection limit. Errors are 1 σ standard deviation from counting statistics only.
Completed data are available in Table S7 in supporting information.

nearly the same (Table 6; Fig. 4d). Bulk rock and shock-melt vein of NWA 4898 both have a convex-upward REE pattern with a pronounced LREE depletion and a nearly flat HREE pattern. A moderate negative Eu anomaly with Eu/Eu* ($2 \times Eu_N/[Sm_N + Gd_N]$) ~0.67 is observed for both shock-melt vein and bulk rock (Fig. 4d; the Gd of the bulk rock was estimated from other HREE). Completed major and trace element data for shock-melt vein are available in Tables S6 and S7 in supporting information.

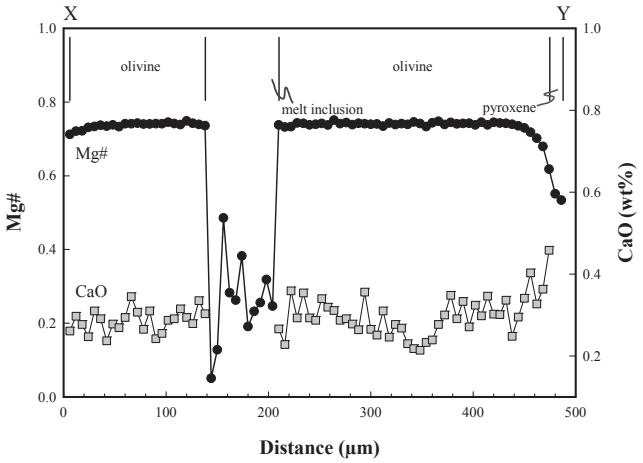

Fig. 5. The composition profile of the olivine phenocryst from X to Y in Fig. 1b, with a step size of 6 μm. The vertical lines at the top divide different phases along the profile. The olivine phenocryst has an equilibrium distribution of Mg and Fe in the inner part but an abrupt decrease of Mg# and an increase of CaO content in the outer rim. CaO concentrations of the melt inclusions and pyroxene reaction rims are not shown because they are too high for the scale.

DISCUSSION

Crystallization Sequence and the Origin of Olivine Phenocrysts and the Associated Inclusions

Euhedral Al-Ti-chromite grains are included in olivine, pyroxene, and maskelynite, which implies that this was the first phase crystallized from the magma. The MELTS simulation program and melting experiments of other high-Al basalts (Walker et al. 1972), whose major element compositions are similar to NWA 4898, both support this interpretation.

Olivine crystallized immediately following Al-Ti-chromite, as shown in the model crystallization sequence (Table 7). The similarity of REE compositions between melt inclusions trapped by Mg-rich olivine crystals and the bulk rock strongly indicates a phenocryst origin for the olivine in NWA 4898 (Fig. 4d). The major element compositions of olivine also support its phenocryst origin. Using the average $K_{d_{\mathrm{Ol-Melt}}}^{\mathrm{Fe-Mg}}$ value of 0.33 for low-Ti basalts (Longhi et al. 1978), the calculated Fo content of an olivine in equilibrium with the whole rock (Mg# = 0.46) is ~72, which generally agrees with the highest Fo measured in olivine phenocrysts (Fo = 74). The chemical zoning of these olivine phenocrysts suggests two stages of crystallization. The first is a relatively slow cooling stage and is characterized by the equilibrated distribution of Mg and Fe in the inner parts of olivine phenocrysts (Fig. 5). The second is a relatively fast cooling stage, which is revealed as an abrupt decrease of Fo along with the increases of CaO and ITE (incompatible trace elements) in the outer rims of olivine phenocrysts (Fig. 5). This is consistent with the ubiquitous variolitic textures in the groundmass of NWA 4898, which formed as a result of nonequilibrium crystallization with a high surface area to volume ratio (Fig. 1c).

The crystallization sequence of plagioclase, ilmenite, and Cr-ulvöspinel could be indicated by Ti and Al contents in pyroxenes, whose Al/Ti ratios vary systematically with their Mg# (Bence and Papike 1972). The Al content in pyroxene increases with Ti at first, indicating plagioclase is not on the liquidus (Fig. 8). When the Al content reaches the maximum (Al is ~0.13 mol%), plagioclase begins to crystallize. At this point, the Al/Ti ratio is ~3 and Mg# is ~0.58. After that, the Al content decreases in the residual melt with increasing Ti content until the crystallization of ilmenite and Cr-ulvöspinel begins, where the Al/Ti ratio is ~2 and Mg# is ~0.5 (Fig. 8b). Subsequently, Ti and Al contents decrease systematically in the residual melt with constant Al/Ti ratio of ~2, while pyroxene, plagioclase, Cr-ulvöspinel, and ilmenite crystallized together until the end. The crystallization sequence of NWA 4898 is as follows: Al-Ti-chromite→ olivine→ pyroxene→ plagioclase→ Cr-ulvöspinel→ ilmenite, which is consistent with the MELTS model calculation.

Inclusions trapped by olivine phenocrysts in basalts may potentially record the initial crystallization conditions (Kent 2008). However, the various types of inclusions in olivine phenocrysts of NWA 4898 were probably entrapped during different crystallization stages. Type A inclusions, which only contain opaque minerals, formed at the earliest stage before olivine crystallization (Fig. 2a). Maskelynite and pyroxene in type B inclusions have moderately evolved and restricted compositions compared to those in the groundmass (Fig. 7). The outlines of type B inclusions indicate that they might have crystallized from pre-existing melt inclusions trapped by olivine phenocrysts (Fig. 2b). Type C inclusions, which consist of glass with minor pyroxene and ilmenite crystals, sometimes located only several hundred microns away from type B inclusions (Figs. 1b and 2c). The contrasting morphologies of the two types of inclusions indicate that they were formed under different cooling conditions. The various mineral phases formed in type B inclusions are a result of slow cooling crystallization after the pre-existing melt was entrapped by olivine phenocrysts (Roedder 1979). The glassy type C inclusions, however, suggest they were quenched. The different cooling history also suggests that type C melt inclusions formed after type B inclusions. The abrupt boundary of Fo and CaO profile between olivine

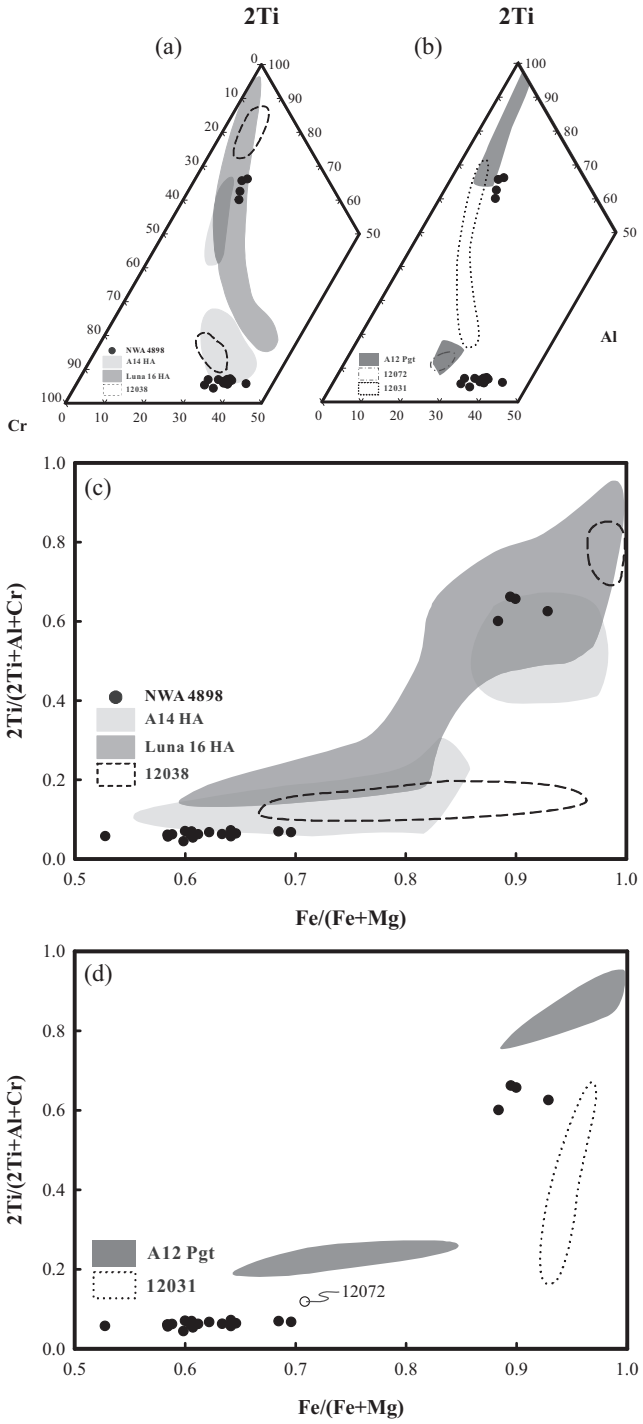

Fig. 6. Panel (a) and (b) are ternary plots of Cr-Al-2Ti (in mol%), while (c) and (d) are plots of Fe/(Fe+Mg) versus 2Ti/(2Ti+Al+Cr) (in mol%) for spinels in NWA 4898. Spinel compositions of 12038, Apollo 14 and Luna 16 high-Al basalts (panel [a] and [c]), normal Apollo 12 pigeonite basalts (i.e., with low alumina content), 12072, and 12031 (panel [b] and [d]) are also plotted for comparison. a) The compositions of Cr-ulvöspinel in NWA 4898 are in the range of Apollo 14 high-Al basalts, whereas Al-Ti-chromite compositions resemble those of Luna 16 high-Al basalts. The Al content in chromite of 12038 is between that of NWA 4898 and Apollo 12 pigeonite basalts. b) The compositions of chromite in 12031 and 12072 do not show high alumina features. c) Spinels in NWA 4898, Apollo 14, and Luna 16 high-Al basalts are all relatively Mg-rich, but Luna 16 spinel is more Ti-rich than that of NWA 4898. Spinel in 12038 has more evolved compositions with both higher Fe# and Ti# compared to those of NWA 4898. d) The compositions of spinel in 12031 and 12072 are more Fe-rich than those of NWA 4898. Data for Apollo 14 high-Al basalts are from El Goresy et al. (1971, 1972), Haggerty (1972a, 1977) and Shervais et al. (1985); those for Luna 16 are from Haggerty (1972b), Grieve et al. (1972), Albee et al. (1972), and Kurat et al. (1976); and those for 12031, 12038, and normal Apollo 12 pigeonite basalts are from Simpson and Bowie (1971), Cameron (1971), Baldridge et al. (1979), Busche et al. (1972), and Arai et al. (1996).

phenocrysts and type C melt inclusion suggests that no significant Mg-Fe exchange between them had occurred and no new olivine crystalized within the melt inclusions (Fig. 5). Therefore, the major and trace element compositions of the melt inclusion could represent the composition of the melt when it was entrapped. Although the major element compositions of type C melt inclusions are heterogeneous, all analysis results have lower Mg# (Fig. 5; 0.19–0.38, with an average of 0.28) than the whole rock (0.46). Compared to the major element compositions, the REE compositions of the melt inclusions are more resistant against postentrapment modification (Kent 2008). The REE abundances of type C inclusions are higher than those of the whole rock, suggesting type C melt inclusions could not represent the parental melt. The fractional crystallization modeling of NWA 4898 suggests that the type C melt inclusions may be entrapped after ~30% fractional crystallization of the parental magma (see the Petrogenesis of NWA 4898 section for details).

Comparison with Other Pristine High-Al Basalts

High-Al basalts have been sampled by several lunar exploration missions. Thus, it is important to seek the relationship between NWA 4898 and other returned high-Al basalts. The Apollo 14 and Luna 16 missions brought back the vast majority of high-Al mare basalts. However, most basalts returned by Apollo 14 were only 1–4 mm in size as clasts in the breccia 14321, although there are two pristine, large basalt samples (14053 and 14072) in the collection. As particles in soils, Luna 16 high-Al basalt samples are also small in size, with the largest B-1 being ~2.5 mm in size. The study of these basalts has been largely hampered by the sample size. The Apollo 12 basalt, 12038, may represent the only feldspathic sample among the basalts returned from Ocean of Storms (Nyquist et al. 1981; Neal et al. 1994).

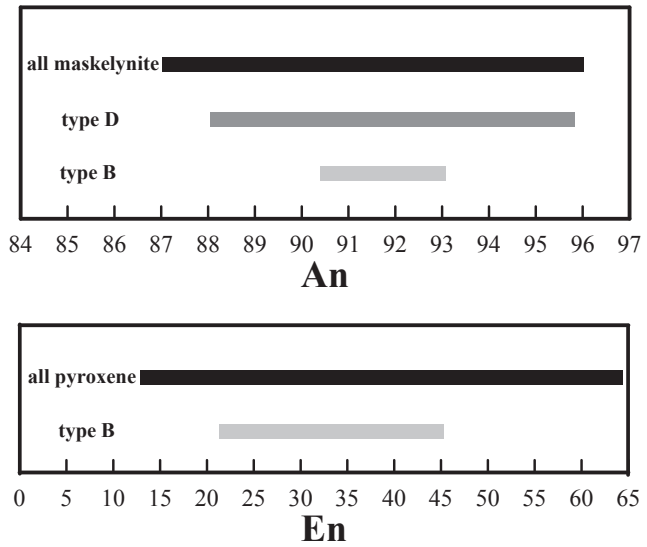

Fig. 7. The ranges of An in maskelynite and En in pyroxene from different types of inclusions compared with all maskelynite and pyroxene in NWA 4898.

Recently, one potential high-Al basalt fragment (60053,2-9) was identified in the Apollo 16 collection (Zeigler et al. 2006). However, this fragment is only ~3 × 1 mm in size and coarse-grained, which results in a large uncertainty about whether the whole rock analysis is representative of its bulk composition. Therefore, only texture and mineral compositions of 60053,2-9 are compared with NWA 4898. Among all lunar meteorites identified so far, NWA 4898 is the only high-Al basalt.

NWA 4898 has a fine-grained, subophitic/ophitic texture, which is similar to most Apollo 14 and Luna 16 high-Al basalts (Reid et al. 1972; Ma et al. 1979; Shervais et al. 1985; Neal et al. 1988, 1989a; Papike et al. 1998). 12038 is medium-grained with a subophitic to intergranular texture (Beaty et al. 1979) and 60053,2-9 is coarse-grained with an equigranular texture (Zeigler et al. 2006). The modal abundance of pyroxene in NWA 4898 is higher than that of other high-Al basalts, but opaque mineral abundance is lower (Table 1).

As one of the first minerals crystallized from the magma, chromite would inherit the chemical signature from its parental magma. Chromite in Apollo 14 and Luna 16 high-Al basalts contains Al_2O_3 content as high as ~25 wt%, compared to less than 13 wt% of other lunar basalts (Papike et al. 1998). This is also true for NWA 4898, with the highest Al_2O_3 content of chromite being ~23 wt%. There are some basalts that also have a high bulk Al_2O_3 content, but the aluminous feature of these rocks may be the result of plagioclase accumulation during a late stage of differentiation. Two such basalts were previously found, 12031 and 12072, both of which contain unusually high bulk Al_2O_3 contents (12.63 and 11.64 wt%, respectively; Beaty et al. 1979; Rhodes et al. 1977) and high modal plagioclase (40.2 and 38.9 vol%, respectively; Neal et al. 1994). They were initially classified as feldspathic basalts (Beaty et al. 1979), but 12031 was later reclassified to be a plagioclase-rich pigeonite basalt based on isotopic evidence (Nyquist et al. 1979; Neal et al. 1994) and 12072 was reclassified as an aluminous olivine basalt with updated bulk rock data (Neal et al. 1994). As one of the earliest crystallized phases, chromite is potentially used to discriminate these two different processes (i.e., inheriting from parental magma or plagioclase accumulation). On the ternary plots of Cr-Al-2Ti (in mol%), the hercynite endmember of chromite in NWA 4898 is comparable with that of Apollo 14 and Luna 16 high-Al basalts (as high as ~45%), whereas that of 12031 and 12072 is much lower and resembles normal Apollo 12 pigeonite basalts (<30%; Figs. 6a and 6b). This suggests that the aluminous feature of NWA 4898, similar to Apollo 14 and Lunar 16 high-Al basalts, is inherited from its parental magma rather than a result of plagioclase accumulation.

Compositions of Al-Ti-chromite in NWA 4898 mostly fall in the low-Ti part of chromite in Apollo 14 high-Al basalts, but are more Ti-depleted than those of Luna 16 high-Al basalts. The compositions of Cr-ulvöspinel fall in the range of Luna 16 high-Al basalts, but are more Al-rich than those of Apollo 14 high-Al basalts (Figs. 6a and 6c). Chromite in Apollo 14 and Luna 16 high-Al basalts has a relatively high Mg content (Haggerty 1972b), which is also observed in NWA 4898 (Fig. 6c). However, chromite in 12072, 12031, and most normal pigeonite basalts contains lower Mg and higher Ti content (Fig. 6d). The spinel compositions of NWA 4898 do not overlap with those of 12038, with the latter being more Ti-rich and marginally less aluminous and more iron-rich (Figs. 6a and 6c). Chromite is not found in 60053,2-9.

Pyroxene in NWA 4898 has a composition range of $En_{12–62}Fs_{25–62}Wo_{11–36}$, with a continuous trend from Mg-rich cores toward Ca-rich mantles and then to Fe-rich rims, overlapping with that of Apollo 14 Group A high-Al mare basalts (Table 2; Fig. 3a; Hagerty et al. 2005). The evolution trend to the Fe-rich pyroxferroite in Luna 16, 12038 was not found in NWA 4898 (Kurat et al. 1976; Beaty et al. 1979). Pyroxene compositions of 60053,2-9 are more evolved than NWA 4898 (Fig. 3b). Symplectite intergrowths of fayalite, hedenbergite, and silica were found in the groundmass of 60053,2-9, which were interpreted to be the breakdown products of pyroxferroite (Zeigler et al. 2006). Plagioclase in NWA 4898 is alkali-depleted, with Or component lower than that of most other high-Al basalts, especially Luna 16

Table 5. Major element compositions (wt%) of shock-melt veins, type C melt inclusions, and bulk rock of NWA 4898, in comparison with other high-Al basalts.

	NWA 4898					Apollo 14 high-Al basalts					
	MV[a]		Type C MI[a]			Group A	Group B	Group C	14072	Luna 16	12038
	Range	Average	Range	Average	BR[b]	BR[c]	BR[c]	BR[c]	BR[d]	BR[e]	BR[f]
SiO_2	45.97–51.24	47.93	47.52–52.93	49.79	46.15	na	na	na	45.2	na	46.59
TiO_2	2.30–3.24	2.76	3.09–4.13	3.47	2.39	1.70–2.92	1.28–2.77	2.22–3.33	2.57	5.13	3.28
Al_2O_3	11.20–13.60	12.28	12.67–15.26	14.16	11.98	11.1–13.1	11.1–14.5	11.5–13.5	11.1	13.3	12.49
Cr_2O_3	0.18–0.52	0.27	0.05–0.17	0.09	0.43	0.33–0.54	0.32–0.59	0.23–0.44	0.51	0.22	
FeO	14.89–18.30	16.93	11.08–13.54	12.65	17.34	15.5–18.4	14.1–19.3	15.5–18.4	17.8	18.6	17.87
MnO	0.14–0.26	0.22	0.14–0.23	0.20	0.25	0.22–0.36	0.16–0.25	0.23–0.40	0.27	0.26	0.26
MgO	5.30–8.26	6.70	2.03–4.50	2.92	8.31	7.8–13.9	7.0–11.9	6.9–9.9	12.2	6.3	6.77
CaO	10.73–12.38	11.58	14.47–16.08	15.35	11.43	9.2–11.9	9.8–12.5	10.2–13.3	9.8	11.8	11.55
Na_2O	0.24–0.41	0.33	0.09–0.19	0.15	0.3	0.32–0.45	0.45–0.65	0.27–0.53	0.32	0.53	0.67
K_2O	0.01–0.11	0.04	0.05–0.15	0.10	na	0.03–0.08	0.08–0.25	0.05–0.30	0.08	0.2	0.07
Total		99.04		98.88	98.58				99.85		99.54
Mg#	0.38–0.48	0.41	0.23–0.38	0.29	0.46	0.46–0.57	0.41–0.56	0.40–0.51	0.55	0.36–0.41	0.4

Abbreviations: na, not analyzed; MV, average of 24 electron microprobe analyses of shock-melt vein; MI, average of seven electron microprobe analyses of melt inclusions; BR, bulk rock; Group A, B, C represent compositional ranges of Group 5&4, 1&2, and 3 high-Al basalts of Dickinson et al. (1985), respectively, as suggested by Neal and Kramer (2006).

Reference sources: a) this study; b) Greshake et al. (2008); c) Dickinson et al. (1985); d) Taylor et al. (1972); e) average of three high-Al basaltic particles from Ma et al. (1979); f) average of four previous independent analyses from Beaty et al. (1979).

Table 6. Trace element compositions (ppm) of shock-melt veins, type C melt inclusions, bulk rock of NWA 4898, in comparison with other high-Al basalts.

	NWA 4898			Apollo 14					
	MV[a]	Type C MI[a]	BR[b]	Group A[c]	Group B[c]	Group C[c]	14072[c]	Luna 16[d]	12038[e]
Sc	66.3 ± 0.2	89.1 ± 0.4	65.4	63.6	61	61.3	51.6	66	50.4
V	na	na	120	138.8	116.9	125	104	77	133
Co	na	na	24.8	34.0	34.5	38.3	39.7	17	32.4
Ni	165 ± 1	168 ± 2	<180	44.3	58.3	76.6	52.4	na	4.42
Y	47.1 ± 0.1	52.5 ± 0.2	na	24.2	77.9	51.7	41.4	na	60
Zr	157.8 ± 0.3	167.9 ± 0.6	145	56.4	316.4	188.2	141	na	185
Ba	70.1 ± 0.2	83.6 ± 0.4	na	35.9	171.6	120.2	107	360	122
La	5.9 ± 0.1	6.8 ± 0.1	4.71	3.1	22.3	11.3	7.8	19.5	12
Ce	18.5 ± 0.1	20.5 ± 0.1	14.8	8.5	59.2	29.8	20.2	53	30.8
Pr	2.98 ± 0.03	3.19 ± 0.05	na	1.27	8.58	4.29	2.87	na	4.64
Nd	16.6 ± 0.1	18.0 ± 0.2	12	6	38.3	20	12.9	43	22
Sm	5.7 ± 0.1	6.4 ± 0.2	4.55	2.02	11.33	6.04	4.21	13.8	6.91
Eu	1.3 ± 0.1	1.3 ± 0.1	0.997	0.59	1.3	0.91	0.98	3.42	1.99
Gd	6.2 ± 0.1	7.3 ± 0.1	na	2.8	13	7.2	5.23	na	9.28
Tb	1.17 ± 0.02	1.42 ± 0.04	1.06	0.55	2.29	1.34	1.02	2.5	1.48
Dy	8.4 ± 0.1	9.6 ± 0.1	na	3.8	14.8	8.9	6.95	16	9.77
Ho	1.79 ± 0.02	2.02 ± 0.04	na	0.91	3.13	1.95	1.46	na	1.94
Er	5.1 ± 0.1	5.7 ± 0.1	na	2.79	8.69	5.68	4.28	na	5.52
Tm	0.76 ± 0.02	0.85 ± 0.03	na	0.44	1.24	0.82	0.64	na	0.74
Yb	5.4 ± 0.1	6.1 ± 0.1	4	2.88	7.73	5.56	4.01	8.2	4.67
Lu	0.76 ± 0.02	0.92 ± 0.04	0.57	0.44	1.09	0.81	0.59	1.16	0.61
Hf	na	na	4.45	1.65	8.15	4.95	3.68	11.2	4.7
Ta	na	na	0.24	0.38	1.11	0.85	0.73	0.6	0.55
Th	na	na	0.44	0.48	2.36	1.6	1.02	1.9	0.61

na, not analyzed; MV, average composition of shock-melt veins; MI, average composition of melt inclusions; BR, bulk rock composition.

Reference sources: a) this study; b) Greshake et al. (2008); c) average of each group samples from Neal and Kramer (2006); d) average of three high-Al basaltic particles from Ma et al. (1979); e) Neal (2001).

Table 7. Crystallization sequence of NWA 4898.

Stage	1	2	3	4	5	6	7	8
Total cryst.	1	5	10	14	24	28	32	44
Crystallizing assemblages (%)								
Olivine	94	96	82	30	30			
Spinel	6	4	3					
Plagioclase					1	10	10	25
Opx			15	40	35			
Cpx						32	65	55
Pigeonite				30	34	58	25	20

Crystallization sequences were derived from a combination of petrographic observations and MELTS simulation program.

(Table 2). Plagioclase in NWA 4898 has a similar $(La/Yb)_N$ ratio to that in Apollo 14 Group A high-Al basalts but with REE concentrations only about half of the latter (Hagerty et al. 2005). Olivine in NWA 4898 has a compositional range nearly overlapping with that of Apollo 14 and Luna 16 high-Al mare basalts. Olivine is rare in 12038 and 60053,2-9 (Table 2). The mineral chemistry of NWA 4898, with its overwhelming similarities to high-Al basalts, suggests that it was derived from a high-Al parental magma by a limited degree of fractional crystallization.

The bulk rock major element compositions of NWA 4898 are distinct from Luna 16 high-Al basalts and 12038, but are similar to Apollo 14 basalts (Fig. 9). Despite the similarities of bulk compositions and mineral chemistry between NWA 4898 and Apollo 14 high-Al basalts, trace element compositions indicate that they were not derived from the same mantle source.

The differences of major element and REE compositions between shock-melt veins and the bulk rock of NWA 4898 suggest that refractory minerals (e.g., chromite) were only partly melted in the veins. Because these minerals are highly depleted in ITE, the partly melting would hardly yield fractionation of ITE in melt veins. ITE ratios of shock-melt veins thus could be used for the bulk rock of NWA 4898, but their absolute abundances should be treated with caution. For example, the average La/Sm ratio of the vein is 1.035, which is the same as that of the bulk rock (1.035) within analytical errors. The ITE ratios were plotted using elements that do not significantly fractionate during low-pressure partial melting or fractional crystallization of the observed phenocryst phases in NWA 4898 and other high-Al basalts (Fig. 10). Basalts with similar ratios would have been derived from a common mantle source (Neal and Kramer 2006). La/Ta versus Zr/Y and Sc/Sm ratios of NWA 4898 fall far away from those of Apollo 14 Group A, C, and 14072, but are close to those of Group B high-Al basalts (Fig. 10), which suggests that NWA 4898 is not derived

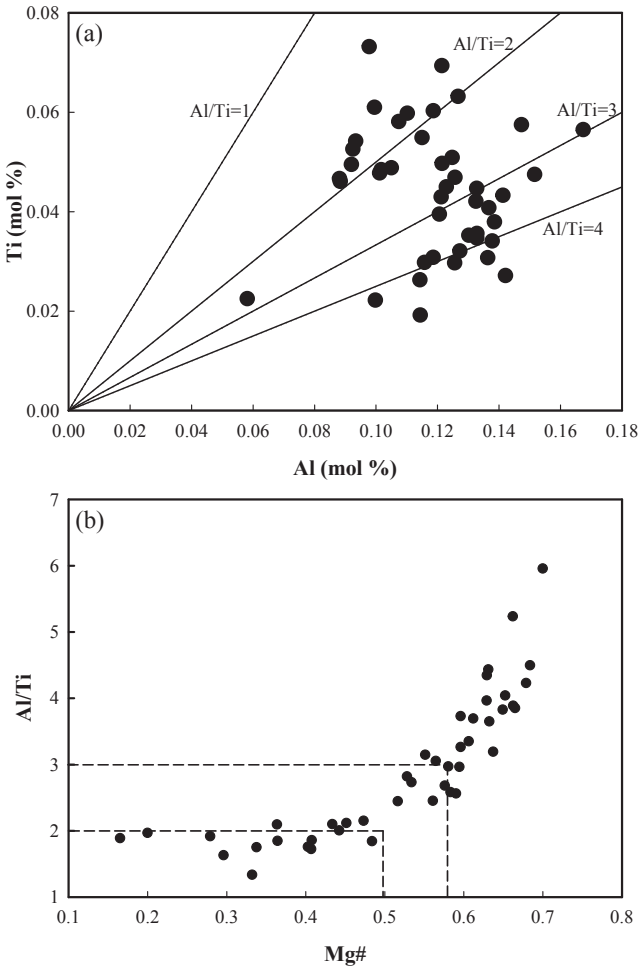

Fig. 8. a) Plots of Al (mol %) versus Ti (mol %) in NWA 4898 pyroxene. b) Mg# versus Al/Ti ratios in NWA 4898 pyroxene.

from the same source with Apollo 14 Group A, C, or 14072 high-Al basalts. The Rb-Sr isotopic and trace element data of Apollo 14 high-Al basalts suggest that source regions for each compositional group can be generated by variable KREEP metasomatism of Group A mantle source (Hui et al. 2013). The ITE ratios of Group B high-Al basalts mantle source can be produced by mixing of ~12% urKREEP and ~88% Group A source (Fig 10; Hui et al. 2013). Although the ITE ratios of NWA 4898 are close to Group B basalts, the mantle source similar to Group B would generate basalts with REE compositions distinct from those of NWA 4898.

The REE abundances of NWA 4898 are similar to those of 14072 and in the range of Apollo 14 Group C (Fig. 11a), but nearly four times less than those of Group B high-Al basalts. The LREE depletion of NWA 4898 is also much more pronounced than those of Apollo 14 high-Al basalts, especially Group B, with

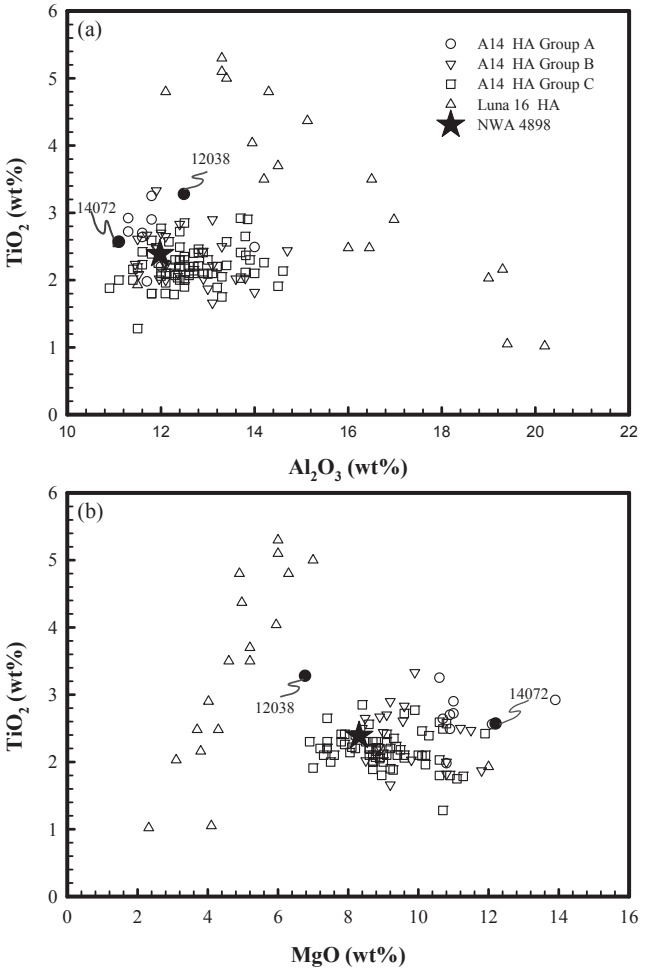

Fig. 9. Variation diagrams for selected whole rock major element compositions for NWA 4898. Apollo 14, 12038, and Luna 16 high-Al basalts are also plotted for comparison. Both (a) and (b) suggest the major element compositions of NWA 4898 are distinct from Luna 16 high-Al basalts and 12038 but fall well within the range of Apollo 14 high-Al basalts. Data for Apollo 14 basalts are from Duncan et al. (1975), Dickinson et al. (1985), Shervais et al. (1985), Neal et al. (1988, 1989b); those for Luna 16 basalts are from Albee et al. (1972), Kurat et al. (1976), and Ma et al. (1979); and those for 12038 are from Neal et al. (1994).

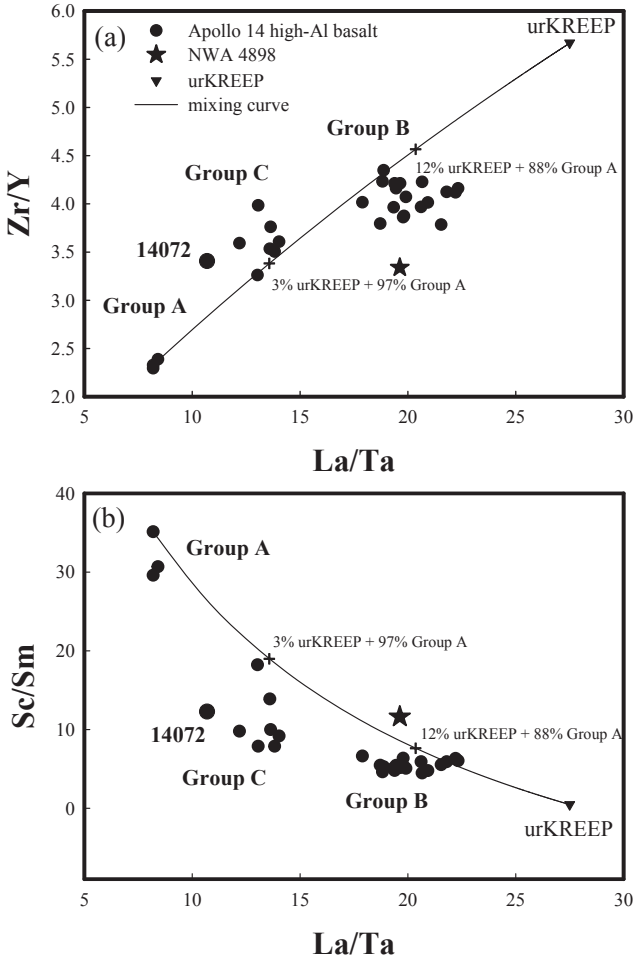

Fig. 10. ITE ratio plots for NWA 4898 and Apollo 14 high-Al basalts with calculated mixing curves between the Group A basalt source and KREEP. Two crosses on the mixing curve represent compositions of 12% urKREEP + 88% Group A and 3% urKREEP +97% Group A, respectively. Both La/Ta versus Zr/Y (a) and La/Ta versus Sc/Sm (b) illustrate that NWA 4898 could not be derived from the mantle sources of Apollo 14 Group A and C high-Al basalts. Data for Apollo 14 high-Al basalts are from Neal and Kramer (2006).

$(La/Sm)_N$ = 0.65 for NWA 4898 compared to 1.16–1.34 for Group B high-Al basalts (Table 6; Fig. 11a) (Dickinson et al. 1985; Neal and Kramer 2006; Neal et al. 1988, 1989b; Shervais et al. 1985). Furthermore, the negative Eu anomaly of NWA 4898 is much less pronounced than those of Apollo 14 Group B, and C, but similar to Group A high-Al basalts (Eu/Eu* = 0.70–0.78 for Group A, 0.25–0.36 for Group B, and 0.37–0.45 for Group C; compared to 0.67 for NWA 4898). The elevated ITE abundances, pronounced LREE enrichment, and strong negative Eu anomaly are all characteristic features for basalts that were contaminated by KREEPy materials. NWA 4898 does not carry a KREEPy signature as most of Apollo 14 high-Al basalts, and could not be generated by partial melting of a mantle source similar to that of Apollo 14 Group B high-Al basalts. NWA 4898 and Apollo 14 high-Al basalts appear to be derived from different mantle sources.

Luna 16 high-Al basalts also show a convex-upward REE pattern (Philpotts et al. 1972; Ma et al. 1979), whose HREE and LREE both display a more fractionated pattern than those of NWA 4898 ($[Gd/Lu]_N$ = 1.59–1.71, $[La/Sm]_N$ = 0.81–1.02). Their REE and most other ITE (e.g., Hf and Th) contents are enriched by a factor of 2–4, and have a slightly smaller

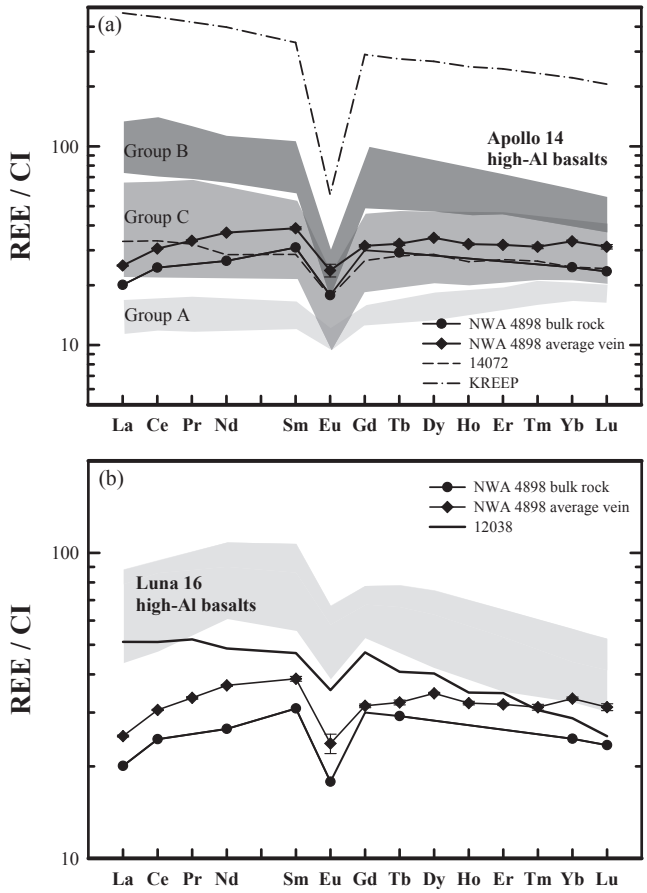

Fig. 11. Comparison of chondrite-normalized REE patterns for NWA 4898 and Apollo 14 (a), 12038 and Luna 16 (b) high-Al basalts. Data for Apollo 14 basalts are from Dickinson et al. (1985), Shervais et al. (1985), Neal et al. (1988, 1989b), and Neal and Kramer (2006); those for Luna 16 are from Philpotts et al. (1972) and Ma et al. (1979); those for 12038 are from Neal (2001); those for KREEP are from Warren and Wasson (1979).

Eu anomaly (Eu/Eu* = 0.72–0.83) than NWA 4898 (Table 6; Fig. 11b). The 12038 has a negative slope REE pattern ($[La/Sm]_N$ = 1.09) from La to Lu, with REE contents slightly higher than NWA 4898 (Fig. 11b; Neal 2001; Nyquist et al. 1981). It could not be related to NWA 4898 by fractional crystallization, because no combination of fractionation of mineral phases observed in these two samples could generate a large variation in LREE pattern but with no significant variations in REE abundances. About 3–5% partially melting of the 12038 mantle source as proposed by Nyquist et al. (1981) could generate the comparable REE abundances as seen in NWA 4898. However, the LREE depletion ([La/Sm] = 0.81–0.88) and the Eu anomaly (Eu/Eu* = 0.87–1.05) of the calculated melt is much less pronounced than that observed in NWA 4898. Therefore, NWA 4898 could not be grouped with any other high-Al basalts and it may have been derived from a separate mantle source that has not been recognized yet from the existing samples.

The age data provide an additional piece of evidence for the difference between NWA 4898 and other high-Al basalts. Apollo 14 high-Al basalts recorded at least three major volcanic events that occurred over a period of ~400 Myr from ~3.9 to ~4.3 Ga (Papanastassiou and Wasserburg 1971; Taylor et al. 1983; Dasch et al. 1987; Nyquist and Shih 1992). Luna 16 high-Al basalts, and 12038 have ages of ~3.39 Ga and 3.34 Ga; respectively (Papanastassiou and Wasserburg 1972; Nyquist et al. 1979, 1981). Gaffney et al. (2008) measured the Rb-Sr age (3.578 ± 0.04 Ga) of NWA 4898. Although this age is only based on a two-point Rb-Sr isochron, it is generally consistent with an independently measured, well defined Ar-Ar age (3.536 ± 0.02 Ga; Fernandes et al. 2009). NWA 4898 is older than the Luna 16 and Apollo 12 high-Al basalts, but younger than Apollo 14 high-Al basalts, which suggests that it recorded an independent magmatic event compared to other high-Al basalts.

Kramer et al. (2008) identified global exposures of high-Al basalts using remote sensing data based on FeO, TiO_2, and Th abundances, and Wu (2012) reevaluated the result by using data with a higher resolution and additional constraints on Al_2O_3 and MgO contents. These authors concluded that high-Al basalts are quite common on the Moon, including regions that are far from Apollo and Luna landing sites.

Parental Magma and Mantle Source of NWA 4898

The whole rock Sm-Nd isotopic composition of NWA 4898 appears to be strongly affected by terrestrial contamination according to Gaffney et al. (2008). However, using the Sm-Nd composition of leached whole rock residue and the age defined by the Rb-Sr system, they found the NWA 4898 mantle source has a $^{147}Sm/^{144}Nd$ ratio of at least 0.34. They thus concluded that NWA 4898 originated from the most depleted mantle source yet identified for the Moon. Among all returned mare basalt samples, Apollo 12 ilmenite basalts and Apollo 17 high-Ti basalts have the highest source $^{147}Sm/^{144}Nd$ values (~0.26 and ~0.27, respectively; Papike et al. 1998; Snyder et al. 1997), corresponding to the most LREE depletion of their parental magma among all mare basalts. Low-Ti basalts, however, only have slightly to moderately super-chondritic $^{147}Sm/^{144}Nd$ ratios (~0.20–0.25; Papike et al. 1998; Shearer et al. 2006), corresponding to moderate LREE depletion of their parental magma. Therefore, the degree of LREE depletion of parental magma could be used as an index for the depletion of mantle source. Because the La/Sm ratio would hardly be altered if there is only a limited degree of fractional crystallization, which is the case for

NWA 4898, the preliminary conclusion of Gaffney et al. (2008) is evaluated in the view of LREE compositions of NWA 4898 parental magma.

Pronounced normal REE zoning was observed in olivine, pyroxenes, and maskelynite, indicating shock metamorphism did not significantly modify REE microdistributions in NWA 4898 (Fig 4; Table 4) (Hsu et al. 2011). Also, no Ce anomalies are observed in individual mafic minerals and melt veins, which suggests the terrestrial weathering was minimal and did not alter the REE compositions of NWA 4898 (Crozaz et al. 2003). In addition, pyroxene appeared early in the crystallization sequence immediately after olivine and chromite. The small-degree (<6%) crystallization of olivine and chromite in NWA 4898 only slightly enriched the REE concentrations of the residual melt, from which pyroxene formed. Therefore, LREE compositions of the melt calculated from the earliest formed pyroxene would closely resemble those of the parental magma for NWA 4898. LREE compositions of the parental magma were estimated by inverting SIMS data of the most primitive pyroxene, using partition coefficients calculated from the equation of McKay et al. (1986). It should be noted that such a calculation involves uncertainties due to the low REE concentrations and the variation of partition coefficients coupled with the chemistry of early formed minerals. Nevertheless, the calculated LREE compositions of the parental magma generally agree with those of the whole rock (Fig. 12).

Parental magma LREE compositions of NWA 4898 are compared with those of Apollo 12 ilmenite basalts and Apollo 17 high-Ti basalts (Fig. 12). It appears that the LREE depletion of the NWA 4898 parental magma is similar to that of Apollo 12 ilmenite basalt parental magma but less pronounced than that of Apollo 17 type B1 high-Ti basalts. This is not consistent with the much higher, potentially contaminated $^{147}Sm/^{144}Nd$ (at least 0.34; Gaffney et al. 2008) of NWA 4898. Therefore, the NWA 4898 parental magma may not have been derived from the most depleted lunar mantle source.

In spite of the aluminous nature of NWA 4898, a significant amount of plagioclase does not need to be present in the source region (Neal and Taylor 1992). High abundance of plagioclase (>10–15%) requires that the source would have a marked positive Eu anomaly (Ridley 1975). The slightly negative Y anomaly (Table 6) in NWA 4898 suggests clinopyroxene would have been retained in the source, which is similar to the case of Apollo 14 high-Al basalts (Neal and Kramer 2006). With the concentration of Sc (~65 ppm) and major element compositions similar to Apollo 14 high-Al basalts, NWA 4898 is believed to have originated from cumulates mainly consisting of olivine, pyroxene, and minor plagioclase.

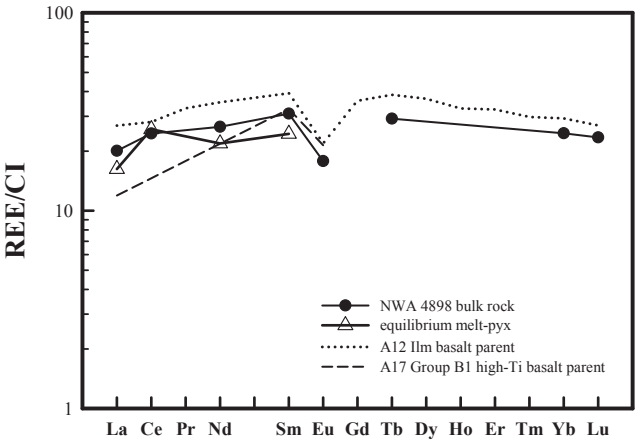

Fig. 12. CI-normalized LREE patterns of NWA 4898 parental magma, which were estimated from the most-primitive pyroxene. The REE patterns of Apollo 12 ilmenite basalts (Snyder et al. 1997) and Apollo 17 high-Ti basalts (Neal et al. 1990) parental magma are also plotted for comparison.

Petrogenesis of NWA 4898

An impact model has been proposed to interpret the unique chemical composition of high-Al basalts. It hypothesizes that high-Al basalts are polymict impact melt rocks formed as mixtures of surface lithologies such as anorthosite, KREEP basalt, etc. (e.g., Snyder and Taylor 2001). Fagan et al. (2013) analyzed olivine compositions from both Apollo 14 impact melt rocks and pristine basalts from Apollo 12, 14, and 17 landing sites and concluded that olivine from impact melts has the highest average Fo and the lowest Co and Mn. MnO is plotted against Fo of olivine in NWA 4898, along with those from Apollo 14 high-Al basalts, impact melts, and Apollo 12 pristine basalts (Fig. 13). Figure 13 clearly illustrates that the composition of olivine from NWA 4898 is distinct from that of impact melts but resembles those of pristine basalts.

Various magmatic models have been proposed for the petrogenesis of high-Al basalts (e.g., Dickinson et al. 1985; Shervais et al. 1985; Neal et al. 1988, 1989a, 1989b; Hagerty et al. 2005; Neal and Kramer 2006; Hui et al. 2011, 2013). They conclusively show that neither different degrees of partial melting of a single source nor a simple fractional crystallization model can account for the trace element characteristics of Apollo 14 high-Al basalts. Various amounts of KREEPy materials could have been involved in the petrogenesis of these basalts (Neal and Kramer 2006; Hui et al. 2011). Incorporation of KREEPy materials may result from (1) a hybridized source with LMO-trapped residual liquid (Hughes et al. 1990), (2) variable urKREEP metasomatism in the high-Al basalt source region (Dickinson et al. 1989; Hui et al. 2013), (3)

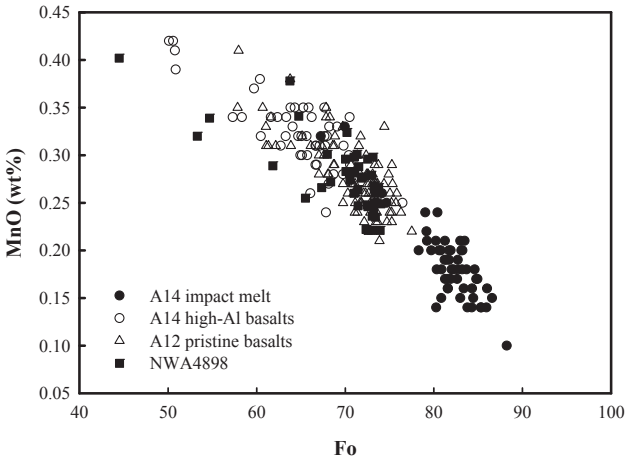

Fig. 13. Mn versus Fo of olivine in NWA 4898, compared with olivines from Apollo 14 high-Al basalts, impact melts, and Apollo 12 pristine basalts (olivine basalts, ilmenite basalts, and pigeonite basalts). It can be seen that compositions of olivine in NWA 4898 are distinct from those in impact melts. Data for olivine of other basalts are all from supplementary materials of Fagan et al. (2013).

assimilating one or multiple ITE-rich component(s) with a primitive magma during its transportation in the lunar crust (e.g., Dickinson et al. 1985; Shervais et al. 1985; Neal et al. 1988; Neal and Kramer 2006), (4) incorporating variable amounts of KREEPy regolith with a low melting point when high-Al lava flowed across the lunar surface (Hui et al. 2011).

The KREEP signature of Apollo 14 high-Al basalts is consistent with the geologic setting of the Apollo 14 landing site. The Apollo 14 mission landed on the Fra Mauro region of Procellarum KREEP Terrane (PKT; Jolliff et al. 2000), which is generally considered to be an ejecta blanket of the Imbrium crater. The returned samples are almost exclusively KREEPy breccia or impact melts, among which soils and breccia fragments from the Cone Crater contain the highest ITE concentrations of all the Apollo samples (e.g., Taylor et al. 1991). Remote sensing data provided evidence that the enrichment of ITE from PKT could extend to a considerable depth (Haskin et al. 2000). This is consistent with the observation that the pristine troctolitic rocks from Apollo 14, whose major element compositions resemble troctolitic rocks collected during other missions, contain radically higher contents of ITE (Warren et al. 1982; Taylor et al. 1991). Most Apollo 14 picritic volcanic glasses, which may represent primary basaltic liquid compositions, also show a unique LREE-enriched pattern, in contrast to those from other landing sites (Shearer et al. 1990; Papike et al. 1998).

In contrast with Apollo 14 high-Al basalts, the trace element compositions of NWA 4898 show no evidence of contamination by KREEPy materials. The good agreement between REE compositions of estimated equilibrium melt from earliest formed minerals and the whole rock composition of NWA 4898 suggests closed-system crystallization environment. The trace element compositions of individual minerals have proven to be more sensitive to the assimilation process, and could record the process that is not evident in the whole rock data (Hui et al. 2011). Therefore, fractional crystallization modeling was undertaken using trace element data from individual minerals.

The bulk composition of NWA 4898 is taken to be the parental melt composition in this model. The crystallization sequences of NWA 4898 were modeled by a combination of petrographic observation and MELTS simulation program (Table 7) (Asimow and Ghiorso 1998; Ghiorso and Sack 1995); the modeling parameters used were the same as those of Neal and Kramer (2006). A fractional crystallization (FC) trajectory was calculated using the equation:

$$C_i^m / C_i^o = F^{(D_i - 1)}$$

where C_i^o and C_i^m are the weight concentration of element i in parental magma and in the residual melt, respectively; D_i is the bulk partition coefficient of element i between minerals and the residual melt. The calculated FC trajectory was compared to the composition of the equilibrium melts of individual minerals that crystallized at different stages. Their agreement would indicate a closed-system fractional crystallization petrogenesis for NWA 4898. Only equilibrated melt of plagioclase was used here because REE partition coefficients of pyroxene are highly dependent on its chemistry (McKay et al. 1986). When Wo varies from 5 mol% to 40 mol% in pyroxene, partition coefficients of REE would increase by an average factor of 25 (Hsu and Crozaz 1996). As a result, even minor re-equilibration of pyroxene would greatly affect the REE contents of the calculated melt. The REE partition coefficients for plagioclase are less sensitive to mineral chemistry (Drake and Weill 1975; Phinney and Morrison 1990), and would remain nearly constant even if being partly re-equilibrated (Hsu and Crozaz 1996). Therefore, the composition of plagioclase could effectively record the assimilation process if any. The partition coefficients used to calculate the equilibrium melt are from regression coefficients of Hui et al. (2011) to further reduce the error induced by chemical variation of plagioclase. Only Ce and Ba were calculated due to the relatively low concentrations and poorly constrained partition coefficients of other measured trace elements in plagioclase (Hui et al. 2011).

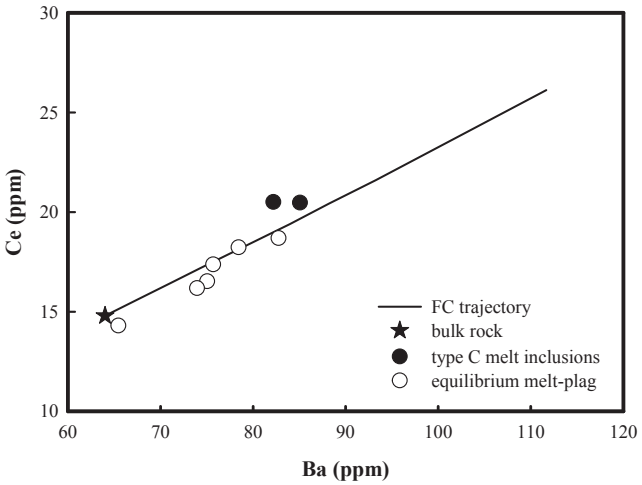

Fig. 14. Fractional crystallization modeling of NWA 4898. The type C melt inclusions and calculated melts that equilibrated with plagioclase, fall on or very close to the FC trajectory of Ba versus Ce, consistent with closed-system fractional crystallization of NWA 4898.

Calculated compositions of equilibrium melt fall on or very close to the FC trajectory (Fig. 14). On the basis of the highly depleted LREE and moderate Eu anomaly, it can be concluded that NWA 4898 was not contaminated by KREEPy materials neither in the mantle source, nor during its ascent to and flowing across the lunar surface. Closed-system fractional crystallization yields the compositions observed in the individual minerals and bulk rock of NWA 4898. The type C melt inclusion compositions were also plotted. If the melt inclusions were residual melts as predicted and if no assimilation of KREEPy materials occurred during the crystallization, they should also fall on the FC trajectory. Figure 14 illustrates that the melt inclusions, as predicted, appear to represent residual melts that were entrapped after ~30% closed-system fractional crystallization of the parental magma.

SUMMARY

NWA 4898 is a unique high-Al basalt among all known basaltic lunar meteorites. It consists predominantly of pyroxene and maskelynite and displays a variolitic texture. Pyroxene compositions ($En_{12–62}Fs_{25–62}Wo_{11–36}$) exhibit a continuous trend from Mg-rich cores toward Ca-rich mantles and then to Fe-rich rims. All plagioclase crystals were converted to maskelynite, and are commonly zoned from An_{96} to An_{87}. Olivine phenocrysts display equilibrated distributions of Mg and Fe in the inner parts (Fo is ~73), but show an abrupt decrease of Fo, coupled with an increase of CaO in the outer rims. All silicate minerals preserve normal REE zoning, which suggests that shock metamorphism did not significantly modify REE microdistributions. Al-Ti-chromite was the first crystallized phase and was overgrown by Cr-ulvöspinel as crystallization proceeded. The aluminous chromite in NWA 4898 indicates that the high aluminum content of NWA 4898 was inherited from its parental magma. This could be used to distinguish the high-Al basalts from those that obtain their high alumina contents through fractional crystallization (e.g., 12031 and 12072).

Four types of inclusions, formed at different crystallization stages, are observed in olivine phenocrysts. Type A inclusions consist of only opaque minerals formed at the earliest stage. Type B inclusions consist of various minerals, which contain moderately evolved but restricted compositions. Type C inclusions are glassy with pyroxene and ilmenite crystals and have evolved compositions relative to the bulk rock. Type D inclusions are texturally between type B and type C inclusions. The contrasting morphologies of these inclusions, coupled with compositional zoning of olivine phenocrysts, suggest NWA 4898 has experienced at least two different cooling stages. The major and trace element compositions of type C inclusions suggest that they do not represent melt that equilibrated with Mg-rich olivine, but rather a residual melt after ~30% closed-system fractional crystallization of the parental magma.

The major element compositions of NWA 4898 resemble Apollo 14 high-Al basalts, but are distinct from Luna 16 high-Al basalts and 12038. Despite the similarities between Apollo 14 high-Al basalts and NWA 4898, the trace element compositions suggest NWA 4898 was derived from a distinct source and had a unique petrogenesis. However, their mantle sources could have similar mineral assemblages.

Based on the difference of olivine compositions between impact melt and pristine mare basalts, we conclude that NWA 4898 has a magmatic origin. The good agreement between the predicted fractional crystallization trajectory and the composition of equilibrated melt of plagioclase suggests closed-system fractional crystallization evolution for NWA 4898. This is distinct from the complicated involvement of KREEPy materials in the petrogenesis of Apollo 14 high-Al basalts.

Acknowledgments—We thank Dr. Steve Elardo and Randy L. Korotev for helpful comments on the earlier version of the manuscript. Constructive reviews by Dr. Clive R. Neal, Amy L. Fagan, and Christine Floss helped to improve this manuscript and are greatly appreciated. This work was supported by the National Natural Science Foundation of China (Grant No.

41273079, 41573059, 41573060) and the Minor Planet Foundation of Purple Mountain Observatory, and FDCT (039/2013/A2).

Editorial Handling—Dr. Randy Korotev

REFERENCES

Albee A., Chodos A., Gancarz A., Haines E., Papanastassiou D., Ray L., Tera F., Wasserburg G., and Wen T. 1972. Mineralogy, petrology, and chemistry of a Luna 16 basaltic fragment, sample B-1. *Earth and Planetary Science Letters* 13:353–367.

Anders E. and Grevesse N. 1989. Abundances of the elements: Meteoritic and solar. *Geochimica et Cosmochimica Acta* 53:197–214.

Arai T., Takeda H., and Warren P. H. 1996. Four lunar mare meteorites: Crystallization trends of pyroxenes and spinels. *Meteoritics & Planetary Science* 31:877–892.

Armstrong J. T. 1982. New ZAF and a-factor correction procedures for the quantitative analysis of individual microparticles. In *Microbeam analysis*, edited by Heinrich K. F. J. San Francisco: San Francisco Press. pp. 175–180.

Asimow P. D. and Ghiorso M. S. 1998. Algorithmic modifications extending MELTS to calculate subsolidus phase relations. *American Mineralogist* 83:1127–1132.

Baldridge W., Beaty D., Hill S., and Albee A. 1979. The petrology of the Apollo 12 pigeonite basalt suite. Proceedings, 10th Lunar and Planetary Science Conference. pp. 141–179.

Beaty D., Hill S., Albee A., and Baldridge W. 1979. Apollo 12 feldspathic basalts 12031, 12038 and 12072—Petrology, comparison and interpretations. Proceedings, 10th Lunar and Planetary Science Conference. pp. 115–139.

Bence A. and Papike J. 1972. Pyroxenes as recorders of lunar basalt petrogenesis: Chemical trends due to crystal-liquid interaction. Proceedings, 3rd Lunar Science Conference. p. 431.

Borg L., Norman M., Nyquist L., Bogard D., Snyder G., Taylor L., and Lindstrom M. 1999. Isotopic studies of ferroan anorthosite 62236: A young lunar crustal rock from a light rare-earth-element-depleted source. *Geochimica et Cosmochimica Acta* 63:2679–2691.

Borg L. E., Connelly J. N., Boyet M., and Carlson R. W. 2011. Chronological evidence that the Moon is either young or did not have a global magma ocean. *Nature* 477:70–72.

Busche F., Prinz M., Keil K., and Bunch T. 1972. Spinels and the petrogenesis of some Apollo 12 igneous rocks. *American Mineralogist* 57:1729–1747.

Cameron E. N. 1971. Opaque minerals in certain lunar rocks from Apollo 12. Proceedings, 2nd Lunar Science Conference. pp. 193–206.

Crozaz G., Floss C., and Wadhwa M. 2003. Chemical alteration and REE mobilization in meteorites from hot and cold deserts. *Geochimica et Cosmochimica Acta* 67:4727–4741.

Dasch E., Shih C. Y., Bansal B., Wiesmann H., and Nyquist L. 1987. Isotopic analysis of basaltic fragments from lunar breccia 14321: Chronology and petrogenesis of pre-Imbrium mare volcanism. *Geochimica et Cosmochimica Acta* 51:3241–3254.

Dickinson T., Taylor G., Keil K., Schmitt R., Hughes S., and Smith M. 1985. Apollo 14 aluminous mare basalts and their possible relationship to KREEP. *Journal of Geophysical Research* 90:C365–C374.

Dickinson T., Taylor G., and Keil K. 1989. Germanium abundances in lunar basalts—Evidence of mantle metasomatism? Proceedings, 19th Lunar and Planetary Science Conference. pp. 189–198.

Drake M. J. and Weill D. F. 1975. Partition of Sr, Ba, Ca, Y, Eu^{2+}, Eu^{3+}, and other REE between plagioclase feldspar and magmatic liquid: An experimental study. *Geochimica et Cosmochimica Acta* 39:689–712.

Duncan A. R., McKay S. M., Stoeser J. W., Lindstrom M. M., Lindstrom D. J., Fruchter J. S., and Goles G. G. 1975. Lunar polymict breccia 14321: A compositional study of its principal components. *Geochimica et Cosmochimica Acta* 39:247–260.

El Goresy A., Ramdohr P., and Taylor L. A. 1971. The geochemistry of the opaque minerals in Apollo 14 crystalline rocks. *Earth and Planetary Science Letters* 13:121–129.

El Goresy A., Taylor L. A., and Ramdohr P. 1972. Fra Mauro crystalline rocks: Mineralogy, geochemistry, and subsolidus reduction of the opaque minerals. Proceedings, 3rd Lunar Science Conference. p. 333.

Elardo S. M., Draper D. S., and Shearer C. K. 2011. Lunar Magma Ocean crystallization revisited: Bulk composition, early cumulate mineralogy, and the source regions of the highlands Mg-suite. *Geochimica et Cosmochimica Acta* 75:3024–3045.

Elardo S. M., McCubbin F. M., and Shearer C. K. 2012. Chromite symplectites in Mg-suite troctolite 76535 as evidence for infiltration metasomatism of a lunar layered intrusion. *Geochimica et Cosmochimica Acta* 87:154–177.

Fagan A. L., Neal C. R., Simonetti A., Donohue P. H., and O'Sullivan K. M. 2013. Distinguishing between Apollo 14 impact melt and pristine mare basalt samples by geochemical and textural analyses of olivine. *Geochimica et Cosmochimica Acta* 106:429–445.

Fernandes V., Korotev R., and Renne P. 2009. ^{40}Ar-^{39}Ar ages and chemical composition for lunar mare basalts: NWA 4734 and NWA 4898 (abstract #1045). 40th Lunar and Planetary Science Conference. CD-ROM.

Gaffney A., Borg L., Depaolo D., and Irving A. 2008. Age and isotope systematics of Northwest Africa 4898, a new type of highly-depleted mare basalt (abstract #1877). 39th Lunar and Planetary Science Conference. CD-ROM.

Ghiorso M. S. and Sack R. O. 1995. Chemical mass transfer in magmatic processes IV. A revised and internally consistent thermodynamic model for the interpolation and extrapolation of liquid-solid equilibria in magmatic systems at elevated temperatures and pressures. *Contributions to Mineralogy and Petrology* 119:197–212.

Greshake A., Irving A., Kuehner S., Korotev R., Gellissen M., and Palme H. 2008. Northwest Africa 4898: A new high-alumina mare basalt from the Moon (abstract #1631). 39th Lunar and Planetary Science Conference. CD-ROM.

Grieve R. A., McKay G. A., and Weill D. F. 1972. Microprobe studies of three Luna 16 basalt fragments. *Earth and Planetary Science Letters* 13:233–242.

Hagerty J. J., Shearer C. K., and Papike J. J. 2005. Petrogenesis of the Apollo 14 high-alumina basalts: Implications from ion microprobe analyses. *Geochimica et Cosmochimica Acta* 69:5831–5845.

Haggerty S. E. 1972a. Apollo 14: Subsolidus reduction and compositional variations of spinels. Proceedings, 3rd Lunar Science Conference. pp. 305–332.

Haggerty S. E. 1972b. Luna 16: An opaque mineral study and a systematic examination of compositional variations of spinels from Mare Fecunditatis. *Earth and Planetary Science Letters* 13:328–352.

Haggerty S. 1977. Apollo 14: Oxide, metal, and olivine mineral chemistries in 14072 with a bearing on the temporal relationships of subsolidus reduction. Proceedings, 8th Lunar Science Conference. pp. 1809–1829.

Haskin L. A., Gillis J. J., Korotev R. L., and Jolliff B. L. 2000. The materials of the lunar Procellarum KREEP Terrane: A synthesis of data from geomorphological mapping, remote sensing, and sample analyses. *Journal of Geophysical Research: Planets* 105:20,403–20,415.

Hess P. C. 1994. Petrogenesis of lunar troctolites. *Journal of Geophysical Research: Planets (1991–2012)* 99:19,083–19,093.

Hsu W. B. and Crozaz G. 1996. Mineral chemistry and the petrogenesis of eucrites.1. Noncumulate eucrites. *Geochimica et Cosmochimica Acta* 60:4571–4591.

Hsu W., Guan Y., Wang H., Leshin L. A., Wang R., Zhang W., Chen X., Zhang F., and Lin C. 2004. The Iherzolitic shergottite Grove Mountains 99027: Rare earth element geochemistry. *Meteoritics & Planetary Science* 39:701–710.

Hsu W., Guan Y., Li S., and Wang Y. 2011. REE microdistributions in NWA 4898: A high-Al mare basalt (abstract #5062). 74th Annual Meeting of the Meteoritical Society. *Meteoritics & Planetary Science* 46:A103.

Hughes S., Neal C., and Taylor L. 1990. Petrogenesis of Apollo 14 high alumina (HA) parental basaltic magma. Proceedings, 21st Lunar and Planetary Science Conference. p. 540.

Hui H., Oshrin J. G., and Neal C. R. 2011. Investigation into the petrogenesis of Apollo 14 high-Al basaltic melts through crystal stratigraphy of plagioclase. *Geochimica et Cosmochimica Acta* 75:6439–6460.

Hui H., Neal C. R., Shih C.-Y., and Nyquist L. E. 2013. Petrogenetic association of the oldest lunar basalts: Combined Rb–Sr isotopic and trace element constraints. *Earth and Planetary Science Letters* 373:150–159.

Jolliff B. L., Gillis J. J., Haskin L. A., Korotev R. L., and Wieczorek M. A. 2000. Major lunar crustal terranes: Surface expressions and crust-mantle origins. *Journal of Geophysical Research: Planets (1991–2012)* 105:4197–4216.

Keil K., Prinz M., and Bunch T. 1971. Mineralogy, petrology, and chemistry of some Apollo 12 samples. Proceedings, 2nd Lunar Science Conference. p. 319.

Kent A. J. 2008. Melt inclusions in basaltic and related volcanic rocks. *Reviews in Mineralogy and Geochemistry* 69:273–331.

Kramer G. Y., Jolliff B. L., and Neal C. R. 2008. Distinguishing high-alumina mare basalts using clementine UVVIS and lunar prospector GRS data: Mare moscoviense and mare nectaris. *Journal of Geophysical Research: Planets* 113:E01002.

Kurat G., Kracher A., Keil K., Warner R., and Prinz M. 1976. Composition and origin of Luna 16 aluminous mare basalts. Proceedings, 7th Lunar Science Conference. pp. 1301–1321.

Longhi J., Walker D., and Hays J. F. 1972. Petrography and crystallization history of basalts 14310 and 14072. Proceedings, 3rd Lunar Science Conference. p. 131.

Longhi J., Walker D., and Hays J. F. 1978. The distribution of Fe and Mg between olivine and lunar basaltic liquids. *Geochimica et Cosmochimica Acta* 42:1545–1558.

Ma M. S., Schmitt R. A., Nielsen R. L., Taylor G. J., Warner R. D., and Keil K. 1979. Petrogenesis of Luna 16 aluminous mare basalts. *Geophysical Research Letters* 6:909–912.

McGee P., Warner J., and Simonds C. 1977. Introduction to the Apollo collections. Part 1: Lunar igneous rocks. *NASA STI/Recon Technical Report N*. pp. 1–96.

McKay G., Wagstaff J., and Yang S. R. 1986. Clinopyroxene REE distribution coefficients for shergottites: The REE content of the Shergotty melt. *Geochimica et Cosmochimica Acta* 50:927–937.

Neal C. R. 2001. Interior of the Moon: The presence of garnet in the primitive deep lunar mantle. *Journal of Geophysical Research: Planets (1991–2012)* 106:27,865–27,885.

Neal C. R. and Kramer G. Y. 2006. The petrogenesis of the Apollo 14 high-Al mare basalts. *American Mineralogist* 91:1521.

Neal C. R. and Taylor L. A. 1992. Petrogenesis of mare basalts: A record of lunar volcanism. *Geochimica et Cosmochimica Acta* 56:2177–2211.

Neal C. R., Taylor L., and Lindstrom M. M. 1988. Apollo 14 mare basalt petrogenesis—Assimilation of KREEP-like components by a fractionating magma. Proceedings, 18th Lunar and Planetary Science Conference. pp. 139–153.

Neal C. R., Taylor L. A., and Patchen A. D. 1989a. High alumina (HA) and very high potassium (VHK) basalt clasts from Apollo 14 breccias. I-Mineralogy and petrology—Evidence of crystallization from evolving magmas. Proceedings, 19th Lunar and Planetary Science Conference. pp. 137–145.

Neal C. R., Taylor L. A., Schmitt R. A., Hughes S. S., and Lindstrom M. M. 1989b. High alumina (HA) and very high potassium (VHK) basalt clasts from Apollo 14 breccias. II-Whole rock geochemistry—Further evidence for combined assimilation and fractional crystallization within the lunar crust. Proceedings, 19th Lunar and Planetary Science Conference. pp. 147–161.

Neal C. R., Taylor L. A., Hughes S. S., and Schmitt R. A. 1990. The significance of fractional crystallization in the petrogenesis of Apollo 17 type A and B high-Ti basalts. *Geochimica et Cosmochimica Acta* 54:1817–1833.

Neal C. R., Hacker M. D., Snyder G. A., Taylor L. A., Liu Y. G., and Schmitt R. A. 1994. Basalt generation at the Apollo 12 site, Part 1: New data, classification, and re-evaluation. *Meteoritics* 29:334–348.

Norman M. D., Borg L. E., Nyquist L. E., and Bogard D. D. 2003. Chronology, geochemistry, and petrology of a ferroan noritic anorthosite clast from Descartes breccia 67215: Clues to the age, origin, structure, and impact history of the lunar crust. *Meteoritics & Planetary Science* 38:645–661.

Nyquist L. E. and Shih C. Y. 1992. The isotopic record of lunar volcanism. *Geochimica et Cosmochimica Acta* 56:2213–2234.

Nyquist L., Shih C.-Y., Wooden J., Bansal B., and Wiesmann H. 1979. The Sr and Nd isotopic record of Apollo 12 basalts: Implications for lunar geochemical evolution. Proceedings, 10th Lunar and Planetary Science Conference. pp. 77–114.

Nyquist L., Wooden J., Shih C.-Y., Wiesmann H., and Bansal B. 1981. Isotopic and REE studies of lunar basalt 12038:

Implications for petrogenesis of aluminous mare basalts. *Earth and Planetary Science Letters* 55:335–355.
Nyquist L. E., Bogard D. D., Shih C. Y., and Wiesmann H. 2002. Negative eNd in anorthositic clasts in Yamato 86032 and MAC88105: Evidence for the LMO? (abstract #1289). 33rd Lunar and Planetary Science Conference. CD-ROM.
Papanastassiou D. A. and Wasserburg G. J. 1971. Rb-Sr ages of igneous rocks from the Apollo 14 mission and the age of the Fra Mauro formation. *Earth and Planetary Science Letters* 12:36–48.
Papanastassiou D. and Wasserburg G. 1972. Rb-Sr age of a Luna 16 basalt and the model age of lunar soils. *Earth and Planetary Science Letters* 13:368–374.
Papike J. J., Ryder G., and Shearer C. K. 1998. Lunar samples. *Reviews in Mineralogy and Geochemistry* 36:5.1–5.234.
Philpotts J., Schnetzler C., Bottino M., Schuhmann S., and Thomas H. 1972. Luna 16: Some Li, K, Rb, Sr, Ba, rare-earth, Zr, and Hf concentrations. *Earth and Planetary Science Letters* 13:429–435.
Phinney W. C. and Morrison D. A. 1990. Partition coefficients for calcic plagioclase: Implications for Archean anorthosites. *Geochimica et Cosmochimica Acta* 54:1639–1654.
Reid J. B. Jr., Taylor G. J., Marvin U. B., and Wood J. A. 1972. Luna 16: Relative proportions and petrologic significance of particles in the soil from Mare Fecunditatis. *Earth and Planetary Science Letters* 13:286–298.
Rhodes J., Brannon J., Rodgers K., Blanchard D., and Dungan M. 1977. Chemistry of Apollo 12 mare basalts: Magma types and fractionation processes. Proceedings, 8th Lunar Science Conference. pp. 1305–1338.
Ridley W. 1975. On high-alumina mare basalts. Proceedings, 6th Lunar Science Conference. pp. 131–145.
Roedder E. 1979. Origin and significance of magmatic inclusions. *Bulletin de Minéralogie* 102:487–510.
Shearer C. K. and Papike J. 2005. Early crustal building processes on the moon: Models for the petrogenesis of the magnesian suite. *Geochimica et Cosmochimica Acta* 69:3445–3461.
Shearer C. K., Papike J. J., Simon S. B., Shimizu N., Yurimoto H., and Sueno S. 1990. Ion microprobe studies of trace elements in Apollo 14 volcanic glass beads: Comparisons to Apollo 14 mare basalts and petrogenesis of picritic magmas. *Geochimica et Cosmochimica Acta* 54:851–867.
Shearer C. K., Hess P. C., Wieczorek M. A., Pritchard M. E., Parmentier E. M., Borg L. E., Longhi J., Elkins-Tanton L. T., Neal C. R., Antonenko I., Canup R. M., Halliday A. N., Grove T. L., Hager B. H., Lee D. C., and Wiechert U. 2006. Thermal and magmatic evolution of the moon. *Reviews in Mineralogy and Geochemistry* 60:365–518.
Shervais J. W., Taylor L. A., and Lindstrom M. M. 1985. Apollo 14 mare basalts—Petrology and geochemistry of clasts from consortium breccia 14321. 15th Lunar and Planetary Science Conference. pp. C375–C395.
Simpson P. and Bowie S. 1971. Opaque phases in Apollo 12 samples. Proceedings, 2nd Lunar Science Conference. p. 207.
Snyder G. and Taylor L. 2001. Oldest mare basalts or impact melts? The role of differential melting of plagioclase in Apollo 14 high-Al basalts. *Meteoritics & Planetary Science Supplement* 36:194.
Snyder G. A., Taylor L. A., and Neal C. R. 1992. A chemical model for generating the sources of mare basalts: Combined equilibrium and fractional crystallization of the lunar magmasphere. *Geochimica et Cosmochimica Acta* 56:3809–3823.
Snyder G. A., Neal C. R., Taylor L. A., and Halliday A. N. 1997. Anataxis of lunar cumulate mantle in time and space. Clues from trace-element, strontium and neodymium isotopic chemistry of parental Apollo 12 basalts. *Geochimica et Cosmochimica Acta* 61:2731–2747.
Taylor S. and Jakes P. 1974. The geochemical evolution of the Moon. Proceedings, 5th Lunar Science Conference. pp. 1287–1305.
Taylor S., Kaye M., Muir P., Nance W., Rudowski R., and Ware N. 1972. Composition of the lunar uplands: Chemistry of Apollo 14 samples from Fra Mauro. Proceedings, 3rd Lunar Science Conference. p. 1231.
Taylor L. A., Shervais J. W., Hunter R. H., Shih C. Y., Bansal B., Wooden J., Nyquist L., and Laul L. 1983. Pre-4.2 AE mare-basalt volcanism in the lunar highlands. *Earth and Planetary Science Letters* 66:33–47.
Taylor G. J., Warren P., Ryder G., Delano J., Pieters C., and Lofgren G. 1991. Lunar rocks. In *Lunar sourcebook: A user's guide to the Moon*, edited by Heiken G., Vaniman D., and French B. M. Cambridge, UK: Cambridge University Press. pp. 183–284.
Taylor L. A., Patchen A., Mayne R. G., and Taylor D. H. 2004. The most reduced rock from the moon, Apollo 14 basalt 14053: Its unique features and their origin. *American Mineralogist* 89:1617–1624.
Walker D., Longhi J., and Hays J. F. 1972. Experimental petrology and origin of Fra Mauro rocks and soil. Proceedings, 3rd Lunar Science Conference. p. 797.
Warner J., Simonds C., and Phinney W. 1976. Genetic distinction between anorthosites and Mg-rich plutonic rocks: New data from 76255. Proceedings, 7th Lunar and Planetary Science Conference. p. 915.
Warren P. H. 1985. The magma ocean concept and lunar evolution. *Annual Review of Earth and Planetary Sciences* 13:201–240.
Warren P. H. and Wasson J. T. 1979. The origin of KREEP. *Reviews of Geophysics* 17:73–88.
Warren P. H., Taylor G. J., Keil K., Marshall C., and Wasson J. T. 1982. Foraging westward for pristine nonmare rocks-Complications for petrogenetic models. Proceedings, 12th Lunar and Planetary Science Conference. pp. 21–40.
Wu Y. 2012. Major elements and Mg# of the Moon: Results from Chang'E-1 Interference Imaging Spectrometer (IIM) data. *Geochimica et Cosmochimica Acta* 93:214–234.
Zeigler R. A., Korotev R. L., Haskin L. A., Jollif B. L., and Gillis J. J. 2006. Petrography and geochemistry of five new Apollo 16 mare basalts and evidence for post-basin deposition of basaltic material at the site. *Meteoritics & Planetary Science* 41:263–284.

SUPPORTING INFORMATION

Additional supporting information may be found in the online version of this article:

Table S1. Electron microprobe analyses (wt%) of olivine in NWA 4898.

Table S2. Electron microprobe analyses (wt%) of pyroxene in NWA 4898.

Table S3. Electron microprobe analyses (wt%) of maskelynite in NWA 4898.

Table S4. Electron microprobe analyses (wt%) of spinel in NWA 4898.

Table S5. Electron microprobe analyses (wt%) of ilmenite and type C melt inclusions in NWA 4898.

Table S6. Electron microprobe analyses (wt%) of shock-melt veins in NWA 4898.

Table S7. Trace element compositions (ppm) of minerals, shock-melt veins, and type C melt inclusions in NWA 4898 analyzed in this study by SIMS.